Journal of Applied Physics ARTICLE pubs.aip.org/aip/jap

Microwave magnetic excitations in U-type hexaferrite $Sr_4CoZnFe_{36}O_{60}$ ceramics

Cite as: J. Appl. Phys. **136**, 073904 (2024); doi: 10.1063/5.0222910
Submitted: 11 June 2024 · Accepted: 3 August 2024 ·
Published Online: 19 August 2024

View Online Export Citation CrossMark

M. Kempa,[1,a)] V. Bovtun,[1] D. Repček,[1,2] J. Buršík,[3] C. Kadlec,[1] and S. Kamba[1]

AFFILIATIONS

[1]Institute of Physics of the Czech Academy of Sciences, Na Slovance 2, Prague 182 00, Czech Republic
[2]Faculty of Nuclear Sciences and Physical Engineering, Czech Technical University in Prague, Břehová 7, Prague 115 19, Czech Republic
[3]Institute of Inorganic Chemistry, Czech Academy of Sciences, Řež near Prague 250 68, Czech Republic

[a)]**Author to whom correspondence should be addressed:** kempa@fzu.cz

ABSTRACT

Microwave (MW) transmission, absorption, and reflection loss spectra of the ferrimagnetic U-type hexaferrite $Sr_4CoZnFe_{36}O_{60}$ ceramics were studied from 100 MHz to 35 GHz at temperatures between 10 and 390 K. Nine MW magnetic excitations with anomalous behavior near ferrimagnetic phase transitions were revealed. They also change under the application of the weak bias magnetic field (0–700 Oe) at room temperature. Six pure magnetic modes are assigned to dynamics of the magnetic domain walls and inhomogeneous magnetic structure of the ceramics, to the natural ferromagnetic resonance (FMR), and to the higher-frequency magnons. Three modes are considered the magnetodielectric ones with the dominating influence of the magnetic properties on their temperature and field dependences. The presence of the natural FMR in all ferrimagnetic phases proves the existence of the non-zero internal magnetization and magnetocrystalline anisotropy. Splitting of the FMR into two components without magnetic bias was observed in the collinear phase and is attributed to a change in the magnetocrystalline anisotropy during phase transition. The high-frequency FMR component critically slows down to phase transition. At room temperature, FMR splitting and essential suppression of the higher-frequency modes were revealed under the weak bias field (300–700 Oe). The highly nonlinear MW response and FMR splitting are caused by the gradual evolution of the polydomain magnetic structure to a monodomain one. The high number of magnetic excitations observed in the MW region confirms the suitability of using hexaferrite $Sr_4CoZnFe_{36}O_{60}$ ceramics as MW absorbers, shielding materials and highly tunable filters.

I. INTRODUCTION

Ferrite materials, called hexaferrites, exhibit a complicated ferrimagnetic arrangement with a hexagonal crystal structure that can be described as stacking sequences of three basic blocks: S $Me_2Fe_4O_8$ (spinel block), where *Me* denotes divalent metal ion; R $[(Ba,Sr)Fe_6O_{11}]^{2-}$ (hexagonal block); and T $(Ba,Sr)_2Fe_8O_{14}$ (hexagonal block). Depending on the stacking sequences of these blocks, hexaferrites are divided into six main types.[1,2] Typical examples are M-type hexaferrite $BaFe_{12}O_{19}$ (stacking sequence SR), Y-type $BaSrCoZnFe_{11}AlO_{22}$ (ST), W-type $SrZnCoFe_{16}O_{27}$ (SSR), Z-type $(Ba,Sr)_3Co_2Fe_{24}O_{41}$ (STSR), X-type $Ba_2Co_2Fe_{28}O_{46}$ (SRS*S*R), and U-type $Sr_4Co_2Fe_{36}O_{60}$ (SRS*R*S*T), where the (*) symbol means that the corresponding block has been turned 180° around the hexagonal c-axis. Due to their unique magnetic properties and economic availability, hexaferrite materials (M-hexaferrites, in particular) are often used in engineering practice, e.g., in refrigerator seal gaskets, microphones, loudspeakers, small motors, clocks, magnetic separators, and in microwave (MW) generators, filters, and absorbers.[3,4]

Hexaferrites are also very interesting from a scientific point of view. Nearly 20 years ago, Kimura found that the conical magnetic structure in Y-hexaferrite induces ferroelectric polarization and that such a multiferroic system exhibits strong magnetoelectric coupling.[5] Similar spin-induced ferroelectricity has been uncovered in a variety of materials with different hexaferrite crystal structures, which often exhibit strong magnetoelectric coupling not only at helium temperatures but also at and above room temperature (RT).[6–8]

Depending on the chemical composition, these materials are ferrimagnetic up to relatively high temperatures of 600–750 K and generally exhibit a set of magnetic phase transitions upon cooling from collinear structures to various conical ones, among which the transverse and alternating longitudinal conical structures are multiferroic.[1] Since hexaferrites exhibit spin-induced ferroelectricity, their magnetoelectric coupling in small magnetic fields is several orders of magnitude higher than in classical $BiFeO_3$, which belongs to type-I multiferroics, where linear magnetoelectric coupling is forbidden due to the incommensurately modulated cycloidal magnetic structure. Only in the field above 18 T does the magnetoelectric coupling in $BiFeO_3$ increase dramatically due to the transition to the canted antiferromagnetic state, where linear magnetoelectricity is already allowed.[9] Static magnetoelectric coupling has so far been studied mainly in hexaferrites with Y- and Z-crystal structures, but multiferroicity has also been reported in some hexaferrites with M-, W-, and U-hexaferrite structures.[10–13] Interestingly, despite the chemical and structural affinities of different hexaferrites, magnetoelectric coupling in Y- and Z-hexaferrite arises from different origins: inverse Dzyaloshinskii–Moriya interaction ($\propto \boldsymbol{S}_i \times \boldsymbol{S}_j$) is responsible for static magnetoelectric coupling in the Y-type hexaferrite, while additional p–d hybridization [$\propto (\boldsymbol{e}_i \cdot \boldsymbol{S}_j)^2 \boldsymbol{e}_i$, where $\boldsymbol{S}_i$ and $\boldsymbol{e}_i$ denote ith spin and the bond direction, respectively] becomes dominant in the Z-type hexaferrite.[14]

A dynamic magnetoelectric coupling can be responsible for the activation of spin excitations in microwave (MW) and terahertz (THz) dielectric spectra. Such excitations are called electromagnons, and in hexaferrites, they are activated, regardless of the type of static magnetoelectric coupling, by exchange striction ($\propto \boldsymbol{S}_i \cdot \boldsymbol{S}_j$).[15–20] One of the characteristic features of an electromagnon is directional dichroism: it means that the reversal of the light incidence direction gives a different electromagnon absorption.[21] Such an effect has mainly been observed in the THz region but has recently been discovered also in the MW region for Y-hexaferrite.[22] In this case, the sign of nonreciprocal MW response could be controlled by the poling electric field, which opens a new avenue for practical applications in magnonics and other future wireless communication technologies. This motivated us to study the microwave properties of $Sr_4CoZnFe_{36}O_{60}$ (CoZnU) with the U-type hexaferrite structure.

Microwave dielectric permittivity and magnetic permeability of various materials with the U-hexaferrite structure have been published more frequently, but practically only at RT and in a limited frequency range up to 6, 12, or maximum 18 GHz.[23–26] In our paper, we focus on CoZnU, which is chemically and structurally related to multiferroic $Sr_4Co_2Fe_{36}O_{60}$ (trigonal space group $R\bar{3}m$).[27] Very recently, we reported that it exhibits a transition from a paramagnetic to a collinear ferrimagnetic structure at $T_{c1} = 635$ K.[28] At $T_{c2} = 305$ K, it transforms into a first conical magnetic structure and at $T_{c3} = 145$ K most probably into a second one, yet not clearly identified.[28] Dielectric studies did not reveal any anomalies near magnetic phase transitions, and magnetoelectric measurements did not find any intrinsic ferroelectric polarization at 10 K.[28] It means that CoZnU is not multiferroic. Here, we report the results of our MW investigations performed up to 50 GHz and down to 10 K, which reveal nine magnetic excitations, including a ferromagnetic resonance (FMR). Most of these excitations show strong temperature dependences near magnetic phase transitions, and we will discuss their origin.

II. EXPERIMENTAL DETAILS

For synthesis of the CoZnU powders and ceramics, the Pechini-type *in situ* polymerizable complex method, relying on the polycondensation reaction (polyesterification) between citric acid and ethylene glycol, was used. Calculated amounts of strontium carbonate ($SrCO_3$), cobalt nitrate ($Co(NO_3)_2{\cdot}6H_2O$), zinc nitrate ($Zn(NO_3)_2{\cdot}6H_2O$), and iron nitrate [$Fe(NO_3)_3{\cdot}9H_2O$; all chemicals from Sigma-Aldrich, 99.9% purity] were dissolved in the distilled water and reacted at 403 K with a solution of a polymer gel formed by the reaction between citric acid ($HOOCCH_2C(OH)$–$(COOH)CH_2COOH$) and ethylene glycol ($HOCH_2CH_2OH$) in water, leading to the voluminous polymer resin. After resin breaking, drying (at 423 K), and charring it (at 623 K) for 24 h, the powder was heat-treated in an oxygen atmosphere at 1488 K for 12 h. Cold isostatic pressing (300 MPa/300 s) and subsequent sintering at 1488 K in oxygen atmosphere led to dense ceramics of the U-phase hexaferrite. X-ray diffraction revealed 97% pure U-hexaferrite with $R\bar{3}m$ space group symmetry and lattice parameters ($a = 5.871$ Å, $c = 112.594$ Å) consistent with the parameters of $Sr_4Co_2Fe_{36}O_{60}$. A detailed description of the CoZnU ceramics preparation, structure, and characterization of its static and dynamic dielectric and magnetic properties can be found in Ref. 28.

In this report, the MW spectroscopy study was performed using two kinds of planar lines: a microstrip line (MSL) and a grounded coplanar waveguide (CPW) with different electromagnetic field distribution and coupling between the sample and line. Our choice is caused by the following reasons. The precise and highly accurate CPW and MSL test boards, which are commercially available and provide propagation of the only quasi-TEM wave without any resonance reflections below 50 GHz,[29] were used. Our study is focused on the absorption bands characterizing the measured material. The frequency range (1–50 GHz), 50 Ohm impedance, geometry, and size of the MSL and CPW test boards correspond well to our experimental facilities and sample size. The propagating quasi-TEM wave provides a good and clear coupling of the electromagnetic field with a sample.

The full set of spectra of the scattering S-parameters (S_{11}, S_{22}, S_{21}, S_{12}, both magnitude and phase)[30] of the Southwest Microwave MSL and CPW 50 GHz test boards[31] loaded with the parallel plate samples (~1 mm thick, ~100 mm^2 surface) at their top (Fig. 1) were recorded in the transmission setup between 100 MHz and 50 GHz on heating from 10 to 390 K in a Janis closed-cycle He cryostat with a temperature rate of 0.5 K/min using the Agilent E8364B network analyzer. The influence of the bias magnetic field H (up to 700 Oe) on the S-parameters spectra, reflection loss, magnetic nonlinearity, and magnetoimpedance effect was studied at RT in the MSL and CPW setups. Reflection loss (S_{11} parameter in the reflection setup)[30] spectra were measured between 100 MHz and 20 GHz using the "short" calibration standard.

The resonance MW measurements were performed using the thin circular disk sample (~0.22 mm thick, ~12 mm in diameter) as a dielectric resonator (DR) with a few resonance frequencies[32] between 8 and 16 GHz, and as a part of the composite dielectric

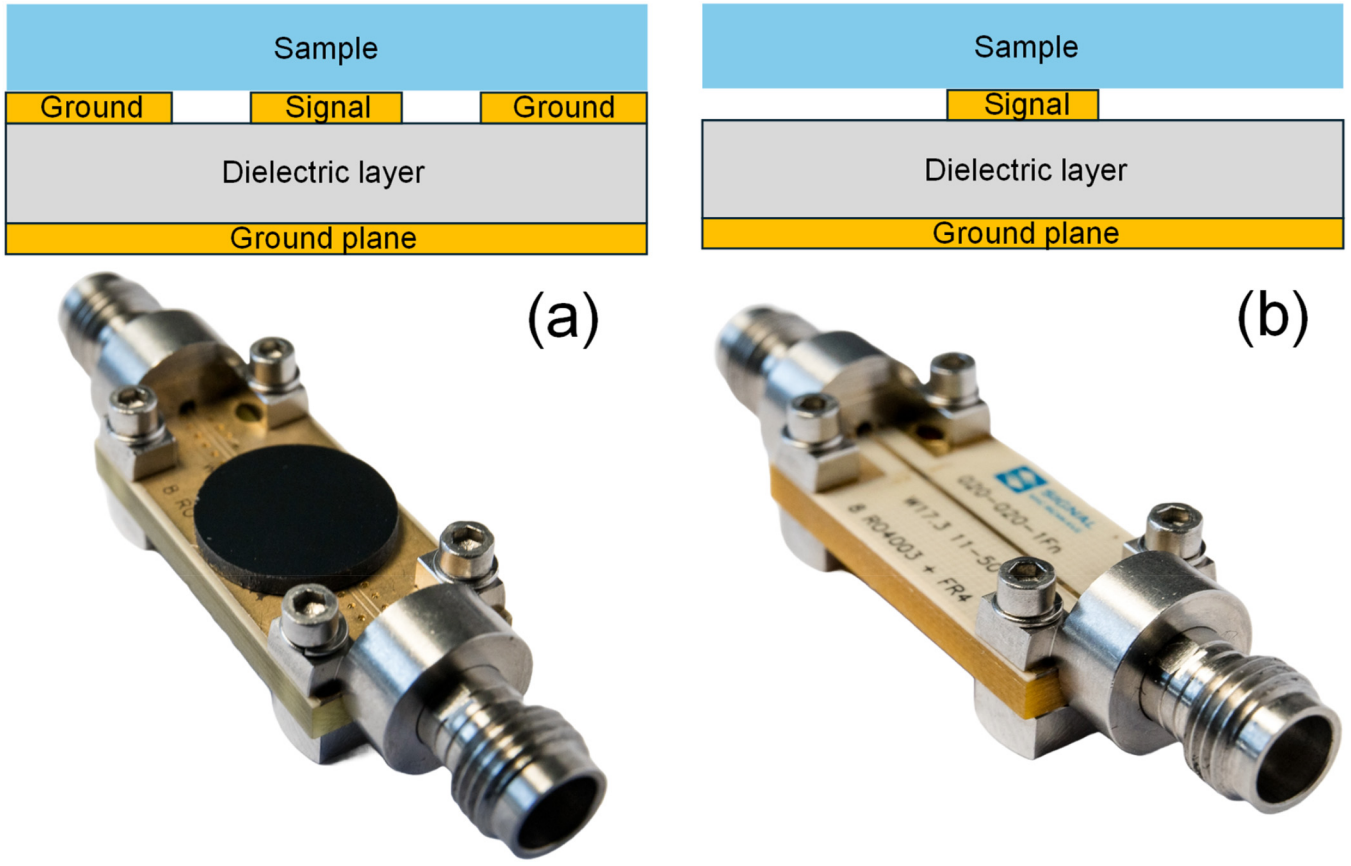

FIG. 1. (a) Schematical cross-sectional view and image of the CPW test board with a sample; (b) schematical cross-sectional view of the MSL test board with a sample and its image without a sample. Samples, signal electrodes, and ground electrodes are shown in the cross-sectional view with different colors. The quasi-TEM wave propagates along the test board, both electrical and magnetic components of the MW field are in the cross-sectional plane.

resonator (CDR)[32–34] at the $TE_{01\delta}$ resonance near 5.8 GHz. The resonators were measured in a cylindrical shielding cavity using the transmission setup with weak coupling by an Agilent E8364B network analyzer during heating from 10 to 390 K with a temperature rate of 0.5 K/min in a Janis closed-cycle He cryostat. In the first case, S_{21} (transmission coefficient) was recorded. In the latter case, the $TE_{01\delta}$ resonance frequency, quality factor, and insertion loss of the base cylindrical dielectric resonator with and without sample were recorded. The effective refractive index and loss tangent of the samples were calculated from the measured parameters of the CDR using MATLAB-based software,[32] accounting for volume fractions of the CDR parts.[33,34]

Time-domain THz spectroscopy was performed by measuring complex sample transmittance using a custom-made spectrometer based on a Ti:sapphire femtosecond laser oscillator (Coherent, Mira, 800 nm, 80 fs, 8 nJ, 76 MHz). Linearly polarized THz pulses were generated by an interdigitated photoconducting antenna (TeraSED, GigaOptics). They were detected by the method of electro-optic sampling in a 1 mm thick ⟨110⟩-oriented ZnTe crystal. The accessible spectral range of the spectrometer is 0.2–3 THz, but our spectra obtained only up to 1.7 THz because the sample becomes opaque at higher frequencies due to strong phonon absorption. Low-temperature measurements were realized in transmission geometry under normal incidence in a helium-flow cryostat (Optistat, Oxford Instruments) with Mylar windows.

Knowing the thickness of the measured ceramics (0.22 mm), we calculated its complex refractive index. In the considered interval, uncertainty was mainly linked to the precision in the measurement of the sample thickness and remained below 3%. The Gouy shift correction was taken into account.[35]

III. BROADBAND MICROWAVE TRANSMISSION AND ABSORPTION

The recorded full set of *S*-parameters of the MSL and CPW loaded with CoZnU ceramics was analyzed (see Fig. S1 in the supplementary material). As the most sensitive and informative parameters, the following were selected and calculated:[30,36,37]

S_{21} magnitude in dB (transmission coefficient Tr), input impedance Z_{in}, and absorption coefficient A. Tr is the most reliable directly measured S-parameter. Its recorded spectra with multiple resonances are similar for the CPW and MSL experiments and show qualitatively similar temperature changes. This similarity is well demonstrated by the comparison of the $Tr(f,T)$ temperature–frequency maps (Figs. 2 and S2 in the supplementary material). In more detail, the temperature evolution of broadband $Tr(f)$ spectra is presented in Fig. 3 for the CPW and in Fig. S3 in the supplementary material for the MSL.

We limited our analysis to the frequency range 1–35 GHz because of too high density of the observed resonances and noise level of the $Tr(f)$ spectra above 35 GHz (see Fig. S1 in the supplementary material). Below 35 GHz, seven well-defined resonance-like or diffuse $Tr(f)$ minima were selected and numbered from T3 to T9 with increasing frequency (here, we continue in the numbering of the excitations seen below 2 GHz in the complex magnetic permeability $\mu^* = \mu' + i\mu''$ published in Ref. 28). Accounting for the observed splitting of the T4 minimum above T_{c2}, its two components are labeled T4a and T4b. The lower-frequency T4a mode joins the T3 one on further heating (above 320 K), the higher-frequency F4b mode critically slows down toward T_{c2} on cooling. All mentioned $Tr(f)$ minima correspond to the MW excitations (transmission modes, T-modes) of the MW line loaded with a CoZnU sample. The same set of T-modes is observed in both CPW and MSL measurements of the same CoZnU sample. Moreover, the temperature evolution of the CPW and MSL T-modes is similar, with a remarkable change of their behavior near CoZnU magnetic phase transitions. T7, T8, and T9 modes are well separated below T_{c2} but become overlapped above T_{c2}, forming one T(7–9) mode. The T4b mode interferes with the T5 and T6 ones above T_{c2} (between 305 and 320 K). As a result, corresponding $Tr(f)$ minima join into the diffuse and asymmetric one, T5 and T6 gradually disappear from the transmission spectra. Consequently, identification of the T3, T4a, T4b, T5, and T6 transmission modes in the collinear phase close to phase transition is complicated. Nevertheless, we carefully followed their temperature evolution: we acquired the transmission spectra with the 1 K step during slow heating (0.5 K per minute). So, we are generally sure about our mode attribution. The T4b mode dominates above T_{c2}. Two modes, T4 (T4a, T4b above T_{c2}) and T7, are characterized by a very pronounced temperature dependence.

The analysis of the transmission coefficient spectra $Tr(f)$ allowed us to observe, reliably separate, and study several MW excitations in the CoZnU hexaferrite. For a better understanding of their nature, the analysis of the absorption coefficient spectra $A(f)$ could be very useful. The $A(f)$ spectrum characterizes the absorption of the electromagnetic energy in a sample. Consequently, $A(f)$ maxima characterize the frequency ranges of the increased absorption of electromagnetic energy due to the interaction with the excitations in the studied material. While the transmission coefficient Tr characterizes the electromagnetic energy which was not absorbed in a sample and not reflected from the sample, the frequencies of the $Tr(f)$ minima are defined by the superposition of the reflection and absorption maxima. Only in

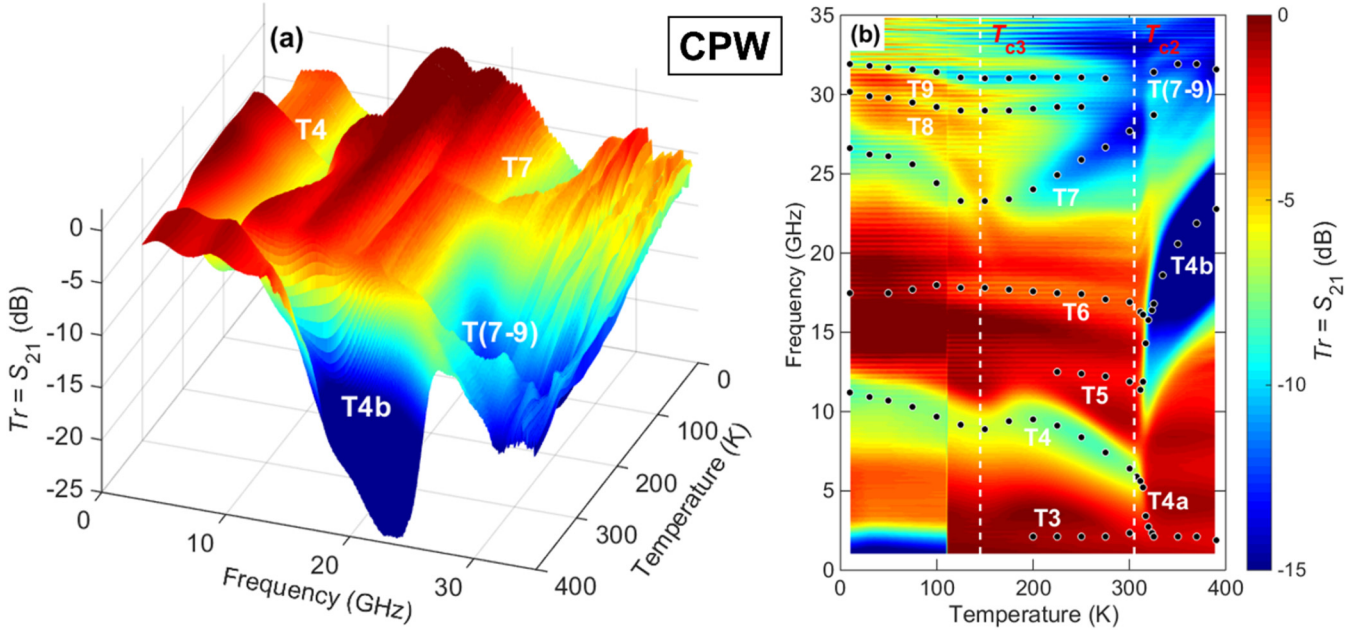

FIG. 2. Temperature–frequency maps of the transmission coefficient Tr (S_{21} magnitude) of CoZnU ceramics obtained using the CPW: (a) in 3D view and (b) as a pseudo-3D color map. Similar maps acquired with the MSL are shown in Fig. S2 in the supplementary material.[36] In (b), points correspond to the main $Tr(f)$ minima shown in Fig. 3. Temperatures of the phase transitions are marked by dashed lines. Apparent jumps of Tr at several temperatures are instrumental artifacts.

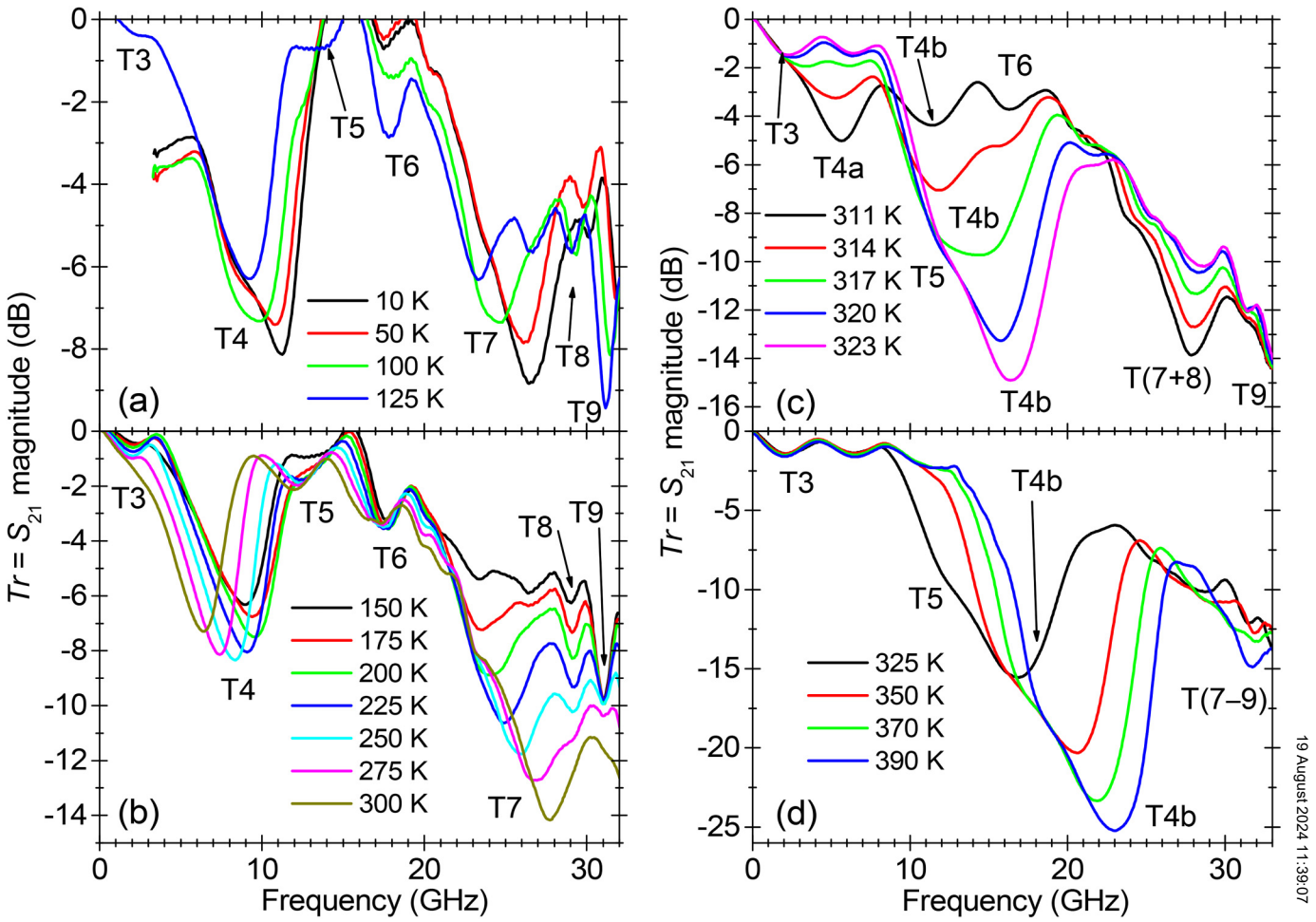

FIG. 3. Broadband spectra of the transmission coefficient Tr (S_{21} magnitude) of the CPW loaded with a CoZnU sample at selected temperatures below T_{c3} (a), between T_{c3} and T_{c2} (b), and above T_{c2} (c) and (d). The main $Tr(f)$ minima are marked T3–T9.

the case where the absorption prevails, the frequencies of the $Tr(f)$ minima correspond to those of the $A(f)$ maxima, both being related to frequencies of the material loss maxima and could be reasonably used for the physical interpretation of the MW excitation, for the study of their microscopic origin. The calculated (see the supplementary material) $A(f)$ spectra are shown for the CPW experiment in Fig. 4 and for the MSL experiment in Fig. S4 in the supplementary material.

Let us note that the deep and broad transmission minima and high-level and broad absorption maxima observed in the MW region evidence the suitability of using the CoZnU hexaferrite ceramics as the microwave absorbing and shielding materials.[3,4]

The absorption spectra are noisier than the transmission ones, nevertheless, seven diffuse $A(f)$ maxima can be recognized below 35 GHz and numbered from A3 to A9 with increasing frequency. These maxima evidence 7 MW excitations (absorption modes, A-modes) of the CoZnU hexaferrite. The same set of A-modes and their similar temperature evolution were derived from both CPW and MSL experiments. The A-mode system corresponds to the T-mode one. The frequencies of A-modes remarkably change near magnetic phase transitions, like those of the T-modes. Therefore, we consider all observed modes (T3–T9, A3–A9) to be related to the magnetic properties and MW excitations (F3–F9) of the CoZnU hexaferrite. We also analyzed the input impedance spectra $Z_{in}(f)$, see Fig. S5 in the supplementary material. The main $Z_{in}(f)$ maxima also correspond to the frequencies of the F3–F9 excitations. The temperature evolution of the F3–F9 excitations is presented in Fig. 5 together with the F1 and F2 magnetic excitations, corresponding to the $\mu''(f)$ maxima from coaxial measurements below 2 GHz and published in Ref. 28.

The transmission spectra of the thin circular disk of the CoZnU sample, measured as a dielectric resonator (DR) in a shielding cavity,[30,32] show a few temperature-dependent resonances with an anomalous behavior near $T_{c2} = 305$ K (see temperature–frequency

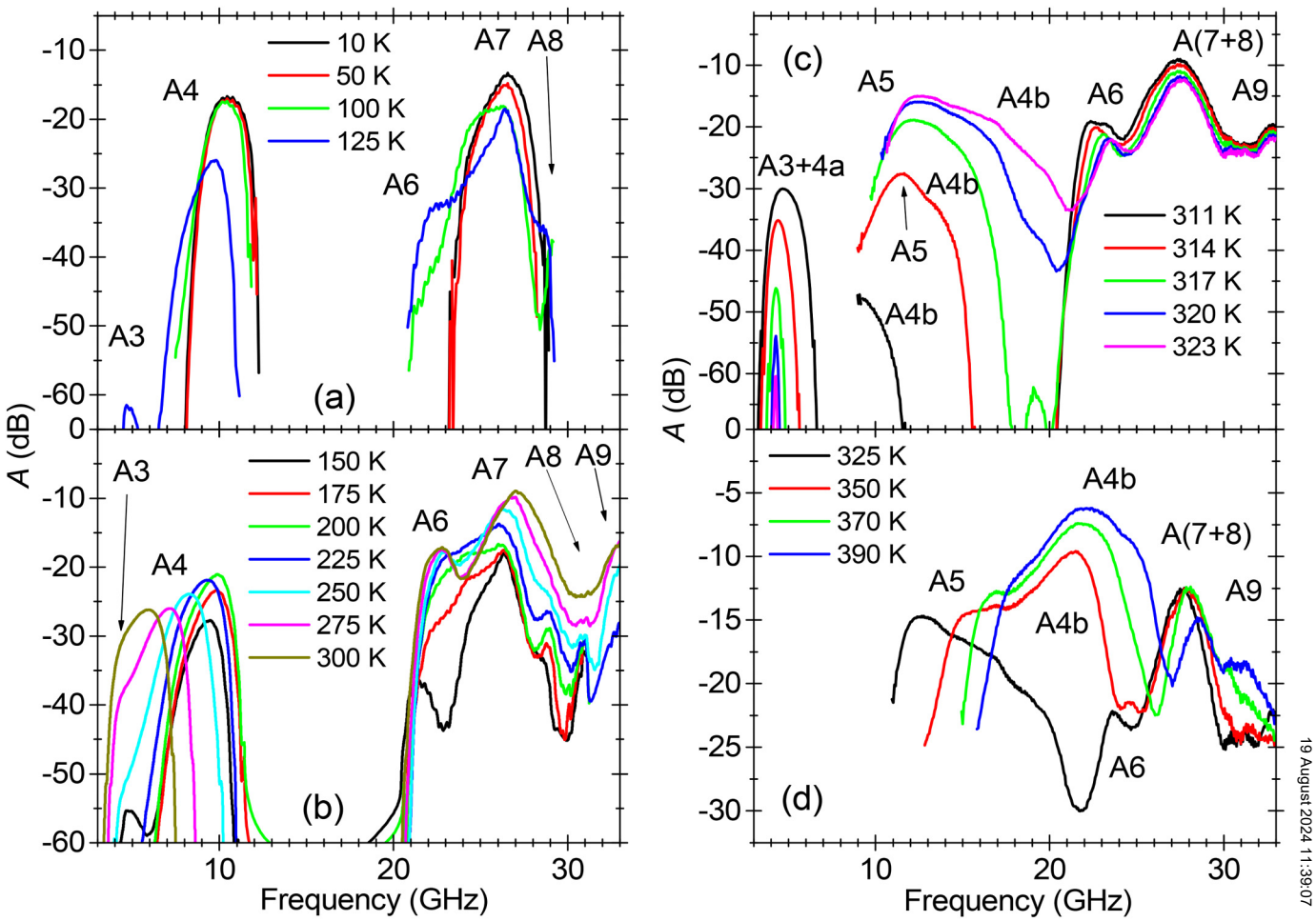

FIG. 4. Broadband spectra of the absorption coefficient A of the CPW loaded with a CoZnU ceramics at selected temperatures below T_{c3} (a), between T_{c3} and T_{c2} (b), and above T_{c2} [(c) and (d)]. The main $A(f)$ maxima are marked A3–A9.

maps in Fig. S5 in the supplementary material). This confirms critical dynamics of the MW excitations in the CoZnU ceramics. We should note that the DR resonance modes are magnetodielectric ones. Their resonance frequencies are defined by the refractive index, i.e., by both the dielectric permittivity and magnetic permeability of the material. As far as the dielectric permittivity is only slightly temperature dependent above 1 GHz, without any anomalies at magnetic phase transitions,[28] temperature dependences of the DR modes, with anomalies near T_{c2}, are related to the critical dependence of the MW magnetic permeability (at least, up to 13 GHz), see also Sec IV.

An essential fact is that independent of the used measurement setup (CPW, MSL, or DR) and of the type of coupling, the main resonance modes in transmission, absorption, or impedance MW spectra exhibit a similar temperature behavior with anomalies near phase transitions. This shows that the MW excitations seen in Fig. 5 are indeed genuine in the CoZnU ceramics, and we will explain their origin in Sec. IV.

IV. TEMPERATURE EVOLUTION OF THE MICROWAVE MAGNETIC EXCITATIONS

No anomalies of the complex dielectric permittivity $\varepsilon^* = \varepsilon' - i\varepsilon''$ (measured between 1 Hz and 1 GHz) were observed near the ferrimagnetic phase transitions at $T_{c3} = 145$ K and $T_{c2} = 305$ K.[28] It is true that at low frequencies, a colossal permittivity was observed in CoZnU,[28] which could mask the dielectric anomaly at spin-induced ferroelectric phase transition, but this colossal permittivity is due to the Maxwell–Wagner relaxations from inhomogeneous conductivity in the CoZnU ceramics. Therefore, the permittivity decreases with increasing frequency, and at 100 MHz or 1 GHz, it already takes intrinsic values of 20–30

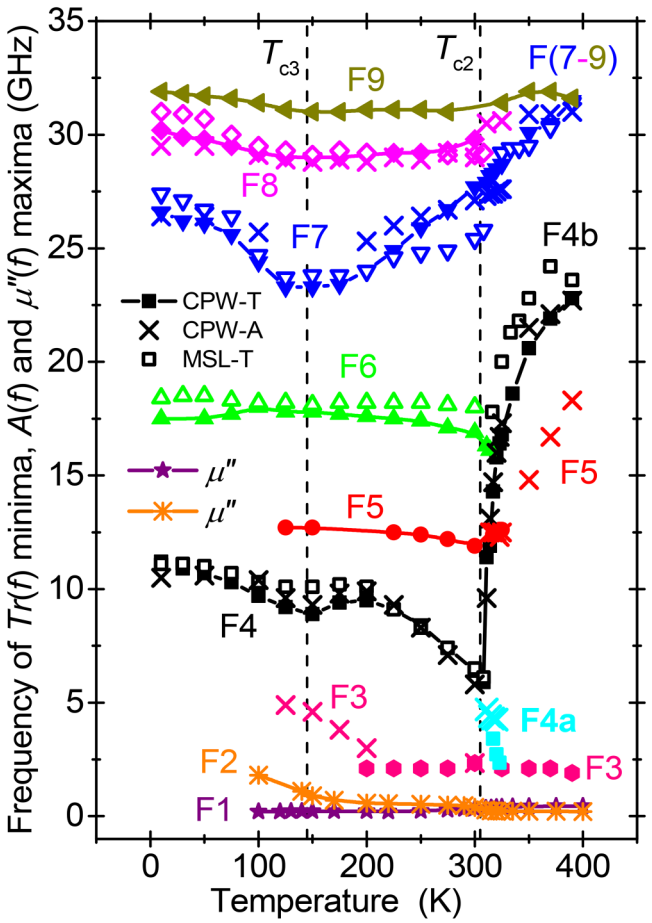

FIG. 5. Temperature evolution of the mean frequencies of the MW excitations F3–F9 corresponding to $Tr(f)$ minima and $A(f)$ maxima of the CPW (lines with filled symbols and crosses, respectively) and MSL (empty symbols) loaded with a CoZnU sample. The mean frequencies of the magnetic excitations F1 and F2, corresponding to the $\mu''(f)$ maxima from coaxial measurements below 2 GHz and published in Ref. 28, are also added.

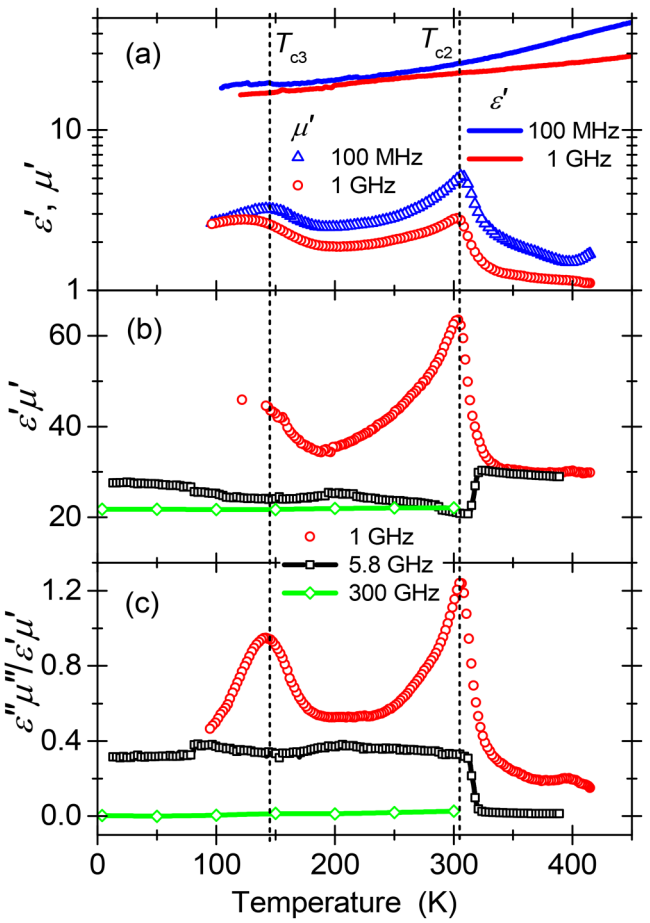

FIG. 6. Temperature dependences of the (a) ε' (lines) and permeability μ' (symbols) at 100 MHz and 1 GHz obtained by coaxial techniques and published in Ref. 28. (b) and (c) $\varepsilon'\mu'$ and $\varepsilon''\mu''/\varepsilon'\mu'$ electromagnetic parameters at 1, 5.8, and 300 GHz.

[see Fig. 6(a)]. The absence of the dielectric anomalies at T_{c2} and T_{c3}, together with the fact that no intrinsic ferroelectric polarization was observed,[28] suggest that CoZnU is not a multiferroic at all temperatures below T_{c1}.

On the other hand, temperature dependences of the permeability $\mu'(T)$ and loss $\mu''(T)$ at 100 MHz and 1 GHz are characterized by the remarkable maxima at T_{c3} and T_{c2}. Below 3 GHz, we separately measured permittivity and permeability using coaxial techniques.[28] At higher frequencies, the dielectric and magnetic parameters cannot simply be distinguished.[32] Our MW measurements, using the MSL, CPW, DR and CDR techniques, as well as the THz one, characterize the full response of the studied material on both electric and magnetic components of the applied electromagnetic field, which depends on both material's permittivity and permeability. Our MSL and CPW techniques revealed the temperature evolution of the main MW excitation in the material, but they do not allow the quantitative estimation of the dielectric and magnetic parameters. The experimental data of the CDR and THz techniques can be analyzed[33,34] using the following mixed electromagnetic parameters: the product $\varepsilon'\mu'$ having the meaning of the square of the refractive index (for negligible index of absorption) and $\varepsilon''\mu''/\varepsilon'\mu'$ as a parameter characterizing electromagnetic losses (loss tangent) in the material.[38] We also calculated $\varepsilon'\mu'$ and $\varepsilon''\mu''/\varepsilon'\mu'$ parameters for 1 GHz (using permittivity and permeability values from coaxial measurements)[28] and show all of them in Figs. 6(b) and 6(c).

The comparison of the 1 GHz $\varepsilon'\mu'$ parameter [Fig. 6(b)] with ε' and μ' [Fig. 6(a)] proves that the $\varepsilon'\mu'$ maxima at $T_{c3} = 145$ K and $T_{c2} = 305$ K are caused by $\mu'(T)$ anomalies. The absence of the dielectric loss ε'' maxima in the 1 GHz temperature dependence[28] evidences an exclusive magnetic nature of the $\varepsilon''\mu''/\varepsilon'\mu'$ loss maxima in the 1 GHz curve [Fig. 6(c)]. Since the 300 GHz $\varepsilon'\mu'$ value is nearly equal to 1 GHz ε', we can conclude that $\mu' \approx 1$ at 300 GHz, and no essential dielectric dispersion (i.e., no dielectric

excitation) takes place in the MW range between 1 and 300 GHz, at least below 300 K. So, the frequency change of the electromagnetic parameters [Figs. 6(b) and 6(c)] is caused only by MW magnetic dispersion. High-frequency permeability dispersion was observed below 1 GHz at temperatures between 100 and 400 K and related to the F1 and F2 modes, which were attributed to dynamics of the domain walls.[28] Above T_{c2}, the main high-frequency permeability dispersion takes place below 500 MHz, values of the F1 and F2 frequencies are lower than 400 MHz, and temperature dependences of the permeability at 500 MHz, 1 GHz, and 1.8 GHz are nearly identical and follow the same Curie–Weiss law. This means that the anomaly in the magnetic permeability seen at magnetic phase transitions must be due to excitations above 1.8 GHz. Therefore, we propose that the critical slowing down of the F4b mode is related to the Curie–Weiss behavior of the 1 GHz permeability. Of course, some magnetic dispersion could be present above 1.8 GHz also and other magnetic excitations could contribute to the 1 GHz permeability besides the F4 mode (most probably, F7). Nevertheless, only the F4b mode critically depends on temperature near T_{c2}.

Note that $\varepsilon'\mu'(T)$ and $\varepsilon''\mu''/\varepsilon'\mu'(T)$ dependences at 5.8 GHz show sharp anomalies near T_{c2}. The $\varepsilon'\mu'(T)$ minimum [in fact, the $\mu'(T)$ minimum] could be explained by the critical slowing down of the mean F4b frequency (Fig. 5) below the frequency of our experiment, like that of the soft mode in ferroelectrics.[39] In the collinear phase above T_{c2}, at temperatures where F4b > 5.8 GHz, $\varepsilon'\mu'$ values at 1 and 5.8 GHz are nearly equal, so the MW magnetic dispersion takes place mainly above 5.8 GHz. In the conical phases below T_{c2}, the higher level of the 5.8 GHz parameters in comparison with the 300 GHz ones also evidences MW magnetic dispersion even above 5.8 GHz. It correlates with the presence of the magnetic excitations (magnons) in the THz range (see Fig. S7 in the supplementary material).

We assume that all MW excitations in Fig. 5 are somehow related to the spin dynamics in CoZnU hexaferrites. MW excitations F4b and F7 with a very pronounced temperature dependence are well observed in both MSL and CPW (A-modes are shown in Fig. 5 only for CPW to preserve the figure clarity). Above T_{c2}, the F7, F8, and F9 excitations join together into the F(7–9) one. The F6 excitation is well resolved only below and near T_{c2} and absent above 315 K. It is characterized by weak temperature dependence. The F5 excitation is better seen as a transmission mode below T_{c2} and as an absorption mode above T_{c2}. It is characterized by weak temperature dependence below T_{c2}, but its frequency [estimated from the $A(f)$ maxima] essentially increases with temperature above T_{c2}. The F3 excitation is well resolved only above 120 K, and its mean frequency is nearly temperature independent above 200 K at the 2 GHz level. Above 320 K, the F4a mode joins F3. The F3 frequency increases below 200 K toward T_{c3}. Let us note that the F3 mean frequency is close to the frequency of the F3 excitation observed at RT in the coaxial experiment,[28] so we consider them as the same excitation.

The F4b mean frequency critically decreases toward T_{c2}. We compare its temperature dependence with that of MW inverse permeability at 1 GHz, which obeys the Curie–Weiss law above T_{c2},

$$\frac{1}{\mu'(T)} = \frac{1}{\left(\mu_L + \frac{C}{T-\theta}\right)}, \quad (1)$$

with parameters: $\mu_L = 1.07$, $C = 8$ K, and $\theta = 305$ K.[28] The temperature dependences of the F4b mean frequency from the CPW experiment (CPW-T in Fig. 5) and of the inverse 1 GHz permeability are shown together in Fig. 7. The F4b mean frequency is proportional to the inverse 1 GHz permeability with a constant factor of 25 GHz at temperatures above T_{c2}. It means that despite the permeability dispersion above 1 GHz, $\mu'(T)$ follows the Curie–Weiss law up to ~22 GHz at high temperatures. Proportionality between the F4b frequency and inverse 1 GHz permeability (Fig. 7) proves the most important contribution of the F4b mode. For that reason, we can claim that the temperature dependence of the 1 GHz permeability above T_{c2} is mainly caused by the temperature change of the F4b frequency. We can, therefore, assign the F4 (F4b) excitation to the critical magnetic excitation, which should correspond to the ferromagnetic resonance (FMR) in the zero bias magnetic field (i.e., natural ferromagnetic resonance). Other two ferrimagnets with the U-hexaferrite structure, $Ba_4Co_{2-3x}Cr_{2x}Fe_{36}O_{60}$ and $Ba_4Zn_{2-x}Co_xFe_{36}O_{60}$, have the FMR frequency at RT near 8[26] and 9.4 GHz, respectively (the latter one in the external magnetic field of 0.3 T).[40] It supports our suggestion that the F4 mode in CoZnU corresponds to the FMR.

Based on the analysis described above, we can propose an explanation for the origin of the observed MW excitations. First, we consider all observed MW modes (F1–F9) to be magnetic. The high number of the magnetic excitations is related to the complex magnetic structure of CoZnU consisting of $(SRS^*R^*S^*T)_3$ magnetic blocks (note that CoZnU contains three formula units with a total of 108 Fe and 3 Co magnetic cations).[27] It is responsible for the formation of many magnon branches in the Brillouin zone[43] and some of the magnons can be activated in MW and THz spectra. The F1, F2, F3, F4 (F4a, F4b), F7, and F8 modes are purely magnetic. Their mean frequencies correspond to the magnetic loss

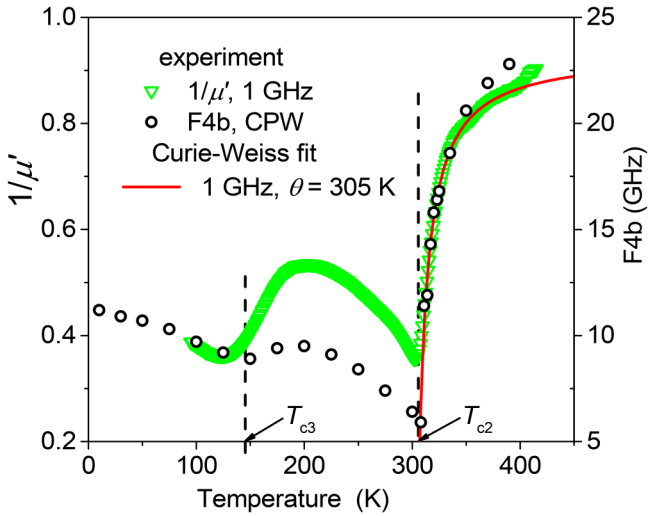

FIG. 7. Temperature dependences of the inverse 1 GHz magnetic permeability with its Curie–Weiss fit [Eq. (1)] above 305 K and eigenfrequency of the F4b magnetic excitation corresponding to FMR.

maxima or MW absorption (MA) maxima caused by the interaction of the electromagnetic field with the magnetic excitations in the CoZnU hexaferrite. (No dielectric excitation takes place in the MW range between 1 and 300 GHz.) The F1 and F2 modes are attributed to dynamics of the magnetic domain walls.[27] The origin of F3 is not so clear, so we can attribute it to dynamics of the inhomogeneous magnetic structure of the non-magnetized hexaferrite ceramics with various orientations of the local magnetic moments of grains and domains, with the presence of grain boundaries.

The F4 mode—natural FMR (at zero magnetic bias)—is a spin wave (magnon) attributed to the collective spin dynamics. High frequency of the natural FMR in all ferrimagnetic phases evidences the existence of the non-zero internal magnetization and magnetocrystalline anisotropy in the previously not magnetized hexaferrite ceramics. The FMR frequency is unambiguously related to the magnetocrystalline anisotropy strength. Splitting of the natural FMR into two components (F4a and F4b) in the collinear phase is caused by a change in the magnetocrystalline anisotropy during the conical to collinear phase transition at T_{c2}.

The higher-frequency pure magnetic modes (F7 and F8) are other magnons of the exchange origin.[41–43] The F5, F6, and F9 modes are magnetodielectric with dominating influence of the magnetic properties on their temperature and field dependences. In the collinear phase, these modes disappear, join the FMR (F5, F6), or overlay with F7 and F8, creating the F(7–9) triplet.

V. MAGNETIC NONLINEARITY OF THE MICROWAVE EXCITATIONS

Essential influence of the weak magnetic bias field H on the RT permeability dispersion, measured in the coaxial setup below 3 GHz, and the bias field dependences of the F1, F2, and F3 mean frequencies responsible for this dispersion, were reported in Ref. 28. It motivated us to study the bias field influence on the MW magnetic excitations above 3 GHz, i.e., on the modes F3–F9. The broadband spectra of the RT transmission of the CPW and MSL loaded with a CoZnU sample at different magnetic bias fields (Fig. 8) evidence the main evolution of the F3–F9 modes with increasing H. The F4 $Tr(f)$ minimum near 6 GHz, corresponding to the FMR, changes non-monotonically. With increasing H, the minimum first becomes sharper, and its depth achieves a maximum of ∼10 dB at ∼300 Oe, then it broadens and its depth decreases (see also Fig. 9). The F4 $Tr(f)$ minimum is asymmetric at low H and becomes symmetric at $H > 400$ Oe. It can be related to the presence of the F3 contribution at lower frequencies, which reduces with increasing H. The F4 frequency non-monotonically decreases with increasing H, with a local maximum at ∼300 Oe corresponding to the deep minimum (Fig. 9).

The field $H > 400$ Oe essentially suppresses all MW modes above 8 GHz, i.e., F5–F9 (see Fig. 8). The F5–F9 modes in MSL are much more pronounced than in CPW (due to stronger coupling of the CoZnU sample with MSL), nevertheless, relatively weak $H = 400$ Oe reduces the depth of their minima down to the 4–5 dB level, similar to that in CPW. Moreover, the peak system of the F7, F8, and F9 modes becomes more damped, and finally, these peaks merge above 300 Oe. Observed suppression of the F5–F9 modes proves their magnetic origin. Their behavior under the magnetic bias reminds their temperature evolution on heating above

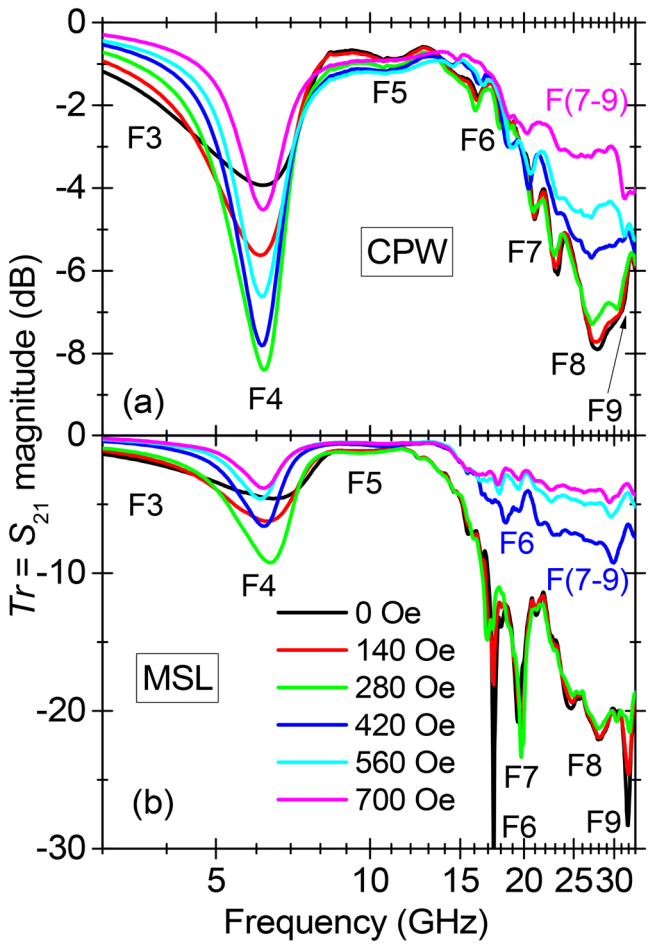

FIG. 8. RT transmission coefficient Tr spectra of the CPW (a) and MSL (b) loaded with a CoZnU sample at different magnetic bias fields. The main $Tr(f)$ minima correspond to the MW excitations F3–F9. Note the log frequency scale.

magnetic phase transition at $T_{c2} = 305$ K (see Fig. 5). Such a high sensitivity of all MW modes to the low bias field could be related to the low (hundreds of Oe) in-plane anisotropy field inducing rotation of the magnetization in the c-plane of hexaferrites.[44]

The RT reflection loss (RL) spectra of the CPW loaded with a CoZnU sample evidence the splitting of the FMR F4 mode into two components (F4a and F4b) under application of the weak bias H field (Fig. 10), which is seen both in RL magnitude and phase. The 15 dB deep diffuse F4 $RL(f)$ minimum becomes sharp and 37 dB deep at $H = 140$ Oe and then splits into the 35 dB deep F4a and 28 dB deep F4a sharp minima at $H = 280$ Oe. At $H = 420$ Oe, the F4a minimum reduces to 20 dB, while the F4a minimum sharpens, and its depth increases to 35 dB. A subsequent increase of the bias field leads to the depth decreasing and widening of both minima. The evolution of the F4 frequency minimum and depth is shown in Fig. 11.

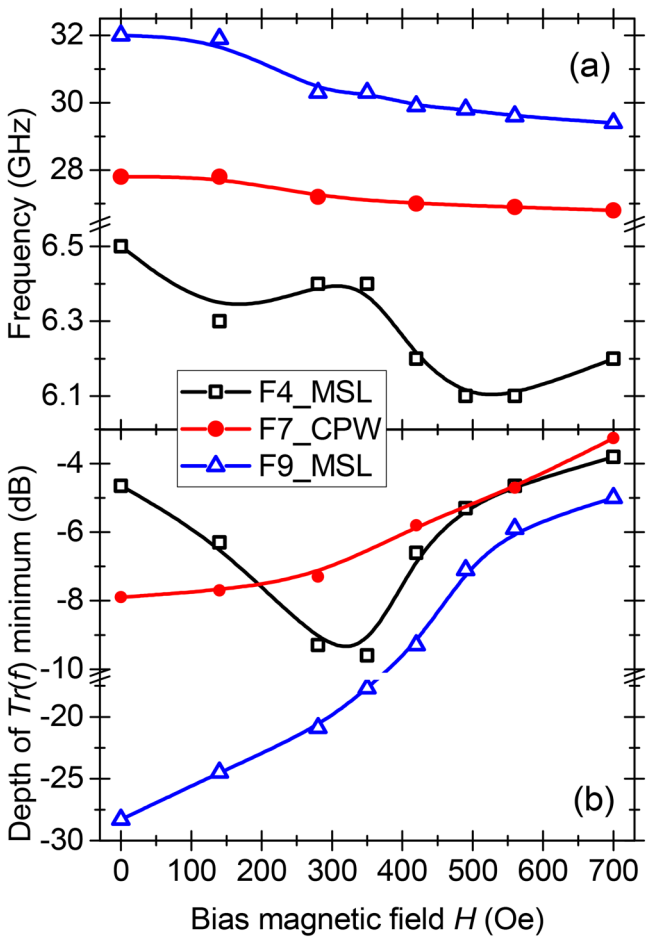

FIG. 9. RT bias magnetic field dependences of frequencies (a) and depths (b) of the $Tr(f)$ minima corresponding to the MW excitations F4, F7, and F9 in CPW or MSL loaded with the CoZnU sample.

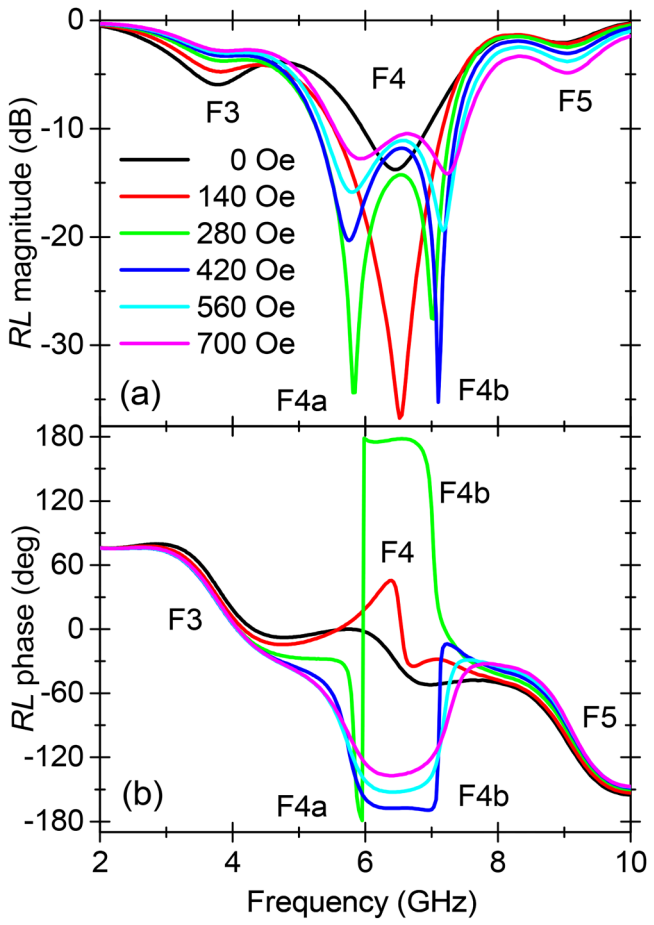

FIG. 10. RT reflection loss RL magnitude (a) and phase (b) spectra below 10 GHz of the CPW loaded with the CoZnU sample at different magnetic bias fields. The RL magnitude minima correspond to the MW modes F3, F4, and F5.

The RL spectra also confirm the presence of the F3 excitation near 4 GHz (Fig. 10) and its dependence on the applied bias field (Fig. 10). The F3 is seen also in the $Tr(f)$ spectra (Fig. 8), but only as a contribution to the asymmetry of the diffuse F4 minimum. In the RL spectra, the F3 minimum is well separated from the F4 one. The application of the bias field suppresses F3 and reduces the depth of its RL minimum from 6 to 2.5 dB [Fig. 11(b)].

Let us note that the RL magnitude is used for the characterization of the electromagnetic MW absorption (MA) of materials:[30,36,37] $MA = -RL$ (dB). So, the $RL(f)$ minima correspond to the $MA(f)$ maxima and, similar to the absorption coefficient $A(f)$ maxima in the transmission experiment (Fig. 4), they are related to the loss maxima in studied materials. The comparison of the room temperature $RL(f)$ minima [Fig. 10(a)] at zero bias field and of 275–300 K $A(f)$ maxima [Fig. 4(b)] allows us to explain the very asymmetric shape of the $A(f)$ maxima by the loss contributions from both F4 and F3 excitations. The loss dependence on the applied bias field proves the magnetic nature of the F3 and F4 excitations.

For quantitative analysis of the CoZnU magnetic nonlinearity, we use a simple method developed for the description of the giant magnetoimpedance effect,[45] i.e., comparison of the H-dependent parameters (Z_{in}) with those under the maximum bias field H_{max} applied in our experiment,

$$\frac{\Delta Z_{in}}{Z_{in}}(\%) = 100\% \times \frac{[Z_{in}(H) - Z_{in}(H_{max})]}{Z_{in}(H_{max})}. \quad (2)$$

The broadband spectra of the input impedance Z_{in} of the CPW loaded with the CoZnU sample are shown in Fig. 12(a). They present remarkable dependence on the bias magnetic field in the whole studied frequency range from 100 MHz to 35 GHz, especially near $Z_{in}(f)$ maxima corresponding to the MW modes F3–F9. The increase of the bias magnetic field suppresses the F3 and F6

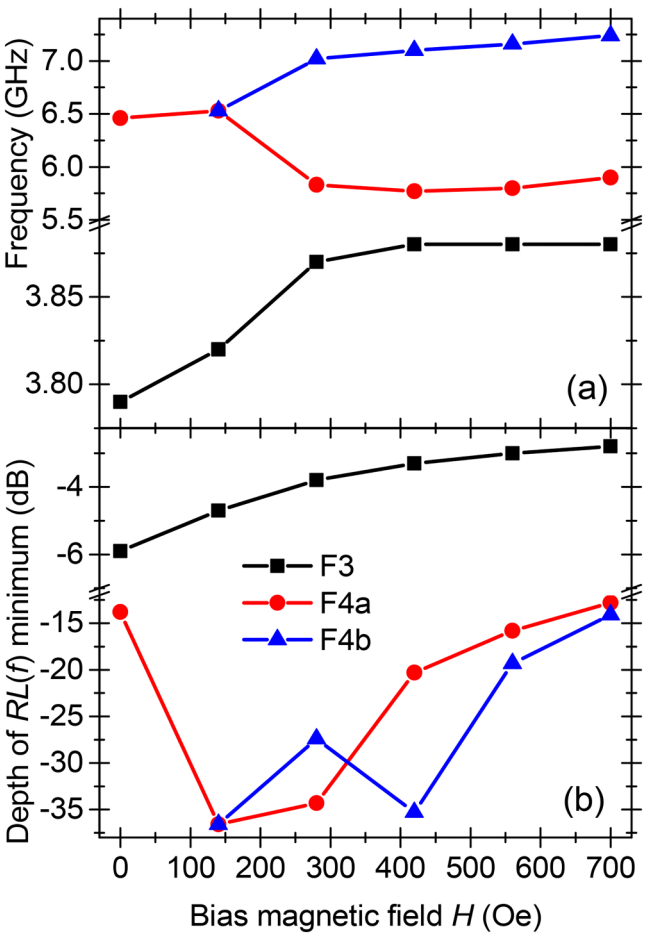

FIG. 11. RT bias magnetic field dependences of the frequencies (a) and depth (b) of the *RL* magnitude minima corresponding to the MW modes F4 and F3 in the CPW loaded with a CoZnU sample.

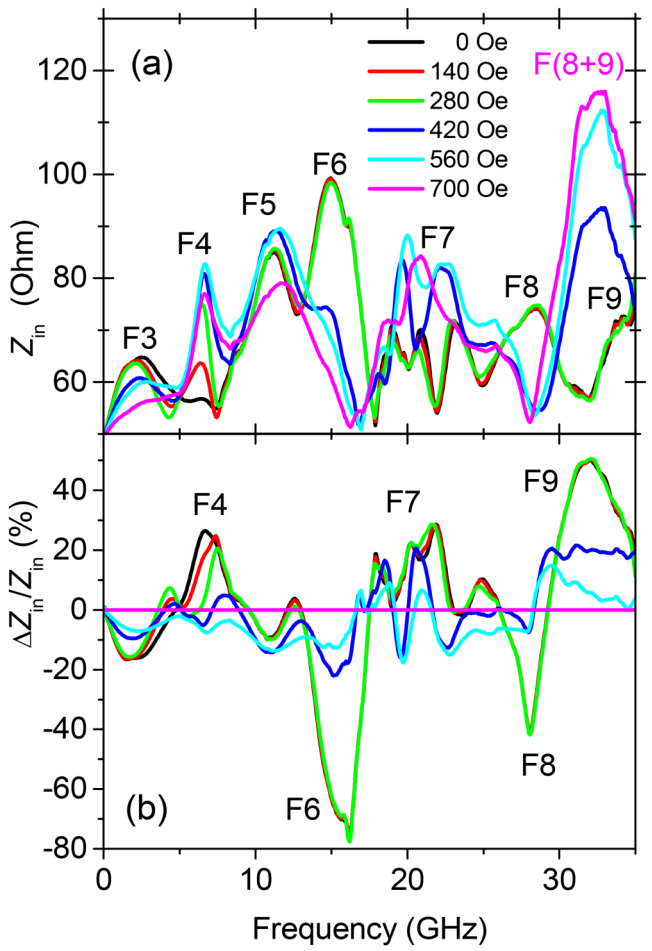

FIG. 12. Broadband spectra of the input impedance Z_{in} of the CPW loaded with the CoZnU sample at different magnetic bias fields (a) and magnetoimpedance effect (b) measured at RT. The main $Z_{in}(f)$ maxima Z3–Z9 correspond to the MW excitations F3–F9.

maxima, nonmonotonically influences the F4 and F7 maxima, and results in increase and emergence of the F8 and F9 maxima. The magnetoimpedance effect [Fig. 12(b)] is the most pronounced near the F4 (>20%), F6 (>70%), and F8–F9 maxima or minima (±50%). Generally, the observed magnetoimpedance effect proves the magnetic nature of the main MW modes between 2 and 35 GHz.

In order to understand why the MW response of the CoZnU ceramics (transmission spectra, reflection loss spectra, and input impedance) essentially changes with increasing temperature or under the application of a weak magnetic bias field $H < 700$ Oe at RT, let us analyze magnetization (discussed in detail in Ref. 28) in a weak field. The temperature dependence of the weak-field magnetization $M_W(T)$ at $H = 100$ Oe [Fig. 13(a)] shows a sharp and substantial anomaly at phase transition from the conical to the collinear phase[28] at $T_{c2} = 305$ K, i.e., close to RT. The main changes of the magnetization $M(H)$ curves at RT and below it, i.e., in the conical magnetic phases, take place in a weak field $H < 700$ Oe and have similar step-like shape and value [Fig. 13(b)]. This step corresponds to the weak-field magnetization M_W.[28] The shape of the $M(H)$ curve at $H < 700$ Oe in the collinear phase, at 348 K, is not step-like; the $M_W(H)$ contribution is smaller. Such $M_W(H)$ temperature evolution corresponds to the $M_W(T)$ curve in Fig. 13(a). The weak-field magnetization M_W and its temperature or field evolution are attributed to the transformation from the polydomain to the monodomain magnetic structure.[28] At RT, i.e., near T_{c2}, the transformation from the polydomain conical structure to the polydomain collinear one with increasing the weak bias field can also contribute to M_W. In addition to M_W, the high-field M_H contribution is seen at $H = 2$–7 kOe in the conical phase below $T_{c2} = 305$ K [Fig. 13(b)], which is attributed to the field-induced transition from the conical to the collinear magnetic phase.[28]

Overall, the highly nonlinear MW response and the high sensitivity of the main magnetic modes of the CoZnU ceramics to the weak magnetic bias field $H < 700$ Oe at RT, as well as the observed

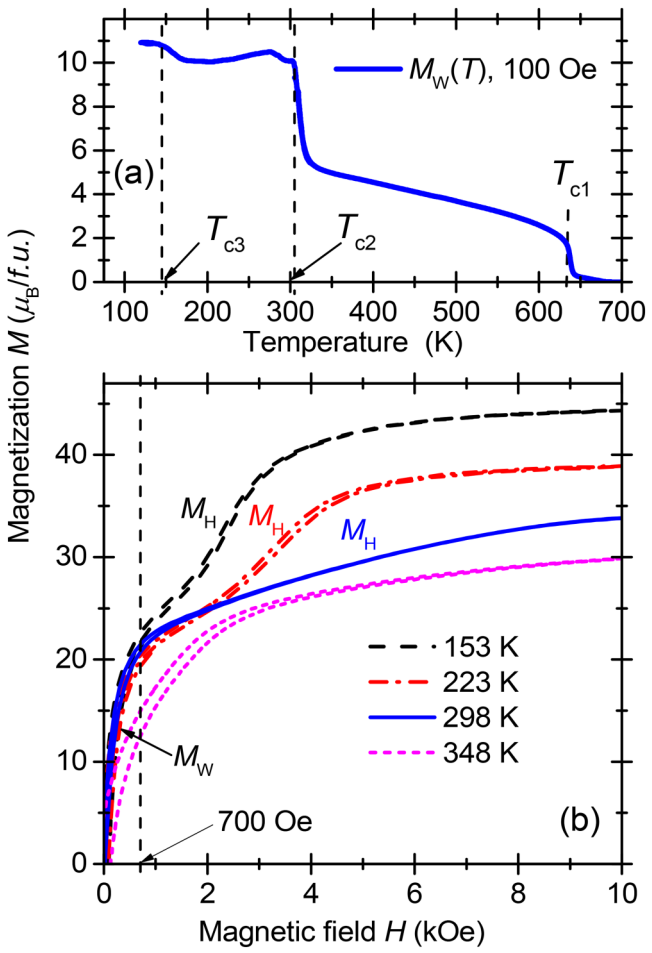

FIG. 13. Temperature dependence of the weak-field magnetization M_w (a). Magnetic field dependences of the magnetization M (b) at selected temperatures. (Data are adopted from Ref. 28.)

FMR mode (F4) splitting, are defined by the weak-field magnetization M_w caused by the gradual transformation of the conical polydomain magnetic structure to the collinear polydomain magnetic one and to the formation of the monodomain structure. It is not a result of the bias field-induced phase transition that should take place at higher bias fields, above 1.5 kOe. The application of high bias magnetic field up to 10 kOe could reveal the T- and H-evolution of the MW excitation in the monodomain sample and during the monodomanization process. It will be a subject of our next study.

The high nonlinearity under the application of the low magnetic field makes the CoZnU hexaferrite ceramics interesting as a material for the highly tunable MW filters.[3,4]

VI. CONCLUSIONS

We revealed 9 MW magnetic excitations below 35 GHz in the $Sr_4CoZnFe_{36}O_{60}$ hexaferrite ceramics and attributed them to dynamics of the magnetic domain walls and to the magnons and magnetodielectric modes. Anomalous behavior of the magnons was observed near magnetic phase transitions. The lowest-frequency magnon was attributed to the natural FMR. Its high frequency (above 5 GHz in all ferrimagnetic phases) proves the existence of non-zero internal magnetization and magnetocrystalline anisotropy in the previously not magnetized ceramics. Splitting of the FMR into two components without magnetic bias was observed near conical to collinear phase transition and attributed to gradual transformation of the conical spin ordering to the collinear one during phase transition at T_{c2}. The higher-frequency FMR component critically slows down to T_{c2}, especially on cooling in the collinear phase.

FMR splitting was also revealed under low bias (300–700 Oe) at room temperature (i.e., in the conical phase near T_{c2}), as well as at the essential suppression of the higher-frequency magnons. The high sensitivity of the MW response to the weak magnetic bias field was shown to correlate with weak-field magnetization of the CoZnU ceramics. This evidences that FMR splitting under low bias is caused by the gradual transformation of the conical polydomain magnetic structure to the collinear one and is not a result of the bias field-induced phase transition, which should take place at higher bias fields, at least above 1.5 kOe.

The high number of MW magnetic excitations sensitive to the weak magnetic field confirms the suitability of using our U-hexaferrite as MW absorbers, shielding materials, and highly tunable magnetic materials. Our study confirms the reliability and effectivity of both used MW planar line techniques. We suggest that information on the genuine MW magnetic excitations in the U-hexaferrite could be useful for the development of the MW elements based on the other types of the planar lines.

SUPPLEMENTARY MATERIAL

See the supplementary material for additional supporting data from CPW, MSL, resonance, and THz measurements.

ACKNOWLEDGMENTS

This work has been supported by the Czech Science Foundation (Project Nos. 21-06802S and 24-10791S), Grant Agency of the Czech Technical University in Prague (Project No. SGS22/182/OHK4/3 T/14), the Research Infrastructure NanoEnviCz (funded by MEYS CR, Project No. LM2018124), and by Project No. TERAFIT-CZ.02.01.01/00/22_008/0004594, co-financed by European Union and the Czech Ministry of Education, Youth and Sports.

AUTHOR DECLARATIONS

Conflict of Interest

The authors have no conflicts to disclose.

Author Contributions

M. Kempa: Data curation (equal); Formal analysis (equal); Investigation (equal); Writing – review & editing (equal). **V. Bovtun:** Data curation (equal); Formal analysis (equal); Investigation (equal); Writing – original draft (lead);

Writing – review & editing (equal). **D. Repček:** Data curation (equal); Formal analysis (equal); Investigation (equal); Writing – original draft (lead); Writing – review & editing (equal). **J. Buršík:** Data curation (equal); Investigation (equal); Writing – review & editing (equal). **C. Kadlec:** Data curation (equal); Investigation (equal). **S. Kamba:** Conceptualization (lead); Data curation (equal); Funding acquisition (lead); Investigation (equal); Project administration (lead); Writing – original draft (supporting); Writing – review & editing (equal).

DATA AVAILABILITY

The data that support the findings of this study are available from the corresponding author upon reasonable request.

REFERENCES

[1]T. Kimura, "Magnetoelectric hexaferrites," Annu. Rev. Condens. Matter Phys. **3**, 93–110 (2012).
[2]R. C. Pullar, "Hexagonal ferrites: A review of the synthesis, properties and applications of hexaferrite ceramics," Prog. Mater. Sci. **57**, 1191–1334 (2012).
[3]V. G. Harris *et al.*, "Recent advances in processing and applications of microwave ferrites," J. Magn. Magn. Mater. **321**, 2035–2047 (2009).
[4]V. G. Harris, "Modern microwave ferrites," IEEE Trans. Magn. **48**, 1075–1104 (2012).
[5]T. Kimura, G. Lawes, and A. P. Ramirez, "Electric polarization rotation in a hexaferrite with long-wavelength magnetic structures," Phys. Rev. Lett. **94**, 137201 (2005).
[6]S. H. Chun, Y. S. Chai, B.-G. Jeon, H. J. Kim, Y. S. Oh, I. Kim, H. Kim, B. J. Jeon, S. Y. Haam, J.-Y. Park, S. H. Lee, J.-H. Chung, J.-H. Park, and K. H. Kim, "Electric field control of nonvolatile four-state magnetization at room temperature," Phys. Rev. Lett. **108**, 177201 (2012).
[7]K. Zhai *et al.*, "Giant magnetoelectric effects achieved by tuning spin cone symmetry in Y-type hexaferrites," Nat. Commun. **8**, 519 (2017).
[8]Y. Kitagawa, Y. Hiraoka, T. Honda, T. Ishikura, H. Nakamura, and T. Kimura, "Low-field magnetoelectric effect at room temperature," Nat. Mater. **9**, 797 (2010).
[9]M. Tokunaga, M. Azuma, and Y. Shimakawa, "High-field study of strong magnetoelectric coupling in single-domain crystals of $BiFeO_3$," J. Phys. Soc. Jpn. **79**, 064713 (2010).
[10]E. H. Na, S. Song, Y.-M. Koo, and H. M. Jang, "Relaxor-like improper ferroelectricity induced by Si·Sj-type collinear spin ordering in a M-type hexaferrite $PbFe_6Ga_6O_{19}$," Acta Mater. **61**, 7705–7711 (2013).
[11]A. V. Trukhanov *et al.*, "Multiferroic properties and structural features of M-type Al-substituted barium hexaferrites," Phys. Solid State **59**, 737–745 (2017).
[12]Y. Q. Song *et al.*, "Spin reorientation transition and near room-temperature multiferroic properties in a W-type hexaferrite $SrZn_{1.15}Co_{0.85}Fe_{16}O_{27}$," J. Appl. Phys. **115**, 093905 (2014).
[13]K. Okumura *et al.*, "Magnetism and magnetoelectricity of a U-type hexaferrite $Sr_4Co_2Fe_{36}O_{60}$," Appl. Phys. Lett. **98**, 212504 (2011).
[14]Y. S. Chai, S. H. Chun, J. Z. Cong, and K. H. Kim, "Magnetoelectricity in multiferroic hexaferrites as understood by crystal symmetry analyses," Phys. Rev. B **98**, 104416 (2018).
[15]N. Kida *et al.*, "Gigantic terahertz magnetochromism via electromagnons in the hexaferrite magnet $Ba_2Mg_2Fe_{12}O_{22}$," Phys. Rev. B **83**, 064422 (2011).
[16]F. Kadlec *et al.*, "Electromagnon in the Z-type hexaferrite $(Ba_xSr_{1-x})_3Co_2Fe_{24}O_{41}$," Phys. Rev. B **94**, 024419 (2016).
[17]F. Kadlec *et al.*, "Electromagnon in the Z-type hexaferrite $(Ba_xSr_{1-x})_3Co_2Fe_{24}O_{41}$," Phys. Rev. B **94**, 024419 (2016).
[18]J. Vít *et al.*, "Electromagnon in the Y-type hexaferrite $BaSrCoZnFe_{11}AlO_{22}$," Phys. Rev. B **97**, 134406 (2018).
[19]S. H. Chun *et al.*, "Electromagnon with sensitive terahertz magnetochromism in a room-temperature magnetoelectric hexaferrite," Phys. Rev. Lett. **120**, 027202 (2018).
[20]H. Shishikura *et al.*, "Electromagnon resonance at room temperature with gigantic magnetochromism," Phys. Rev. Appl. **9**, 044033 (2018).
[21]Y. Tokura, S. Seki, and N. Nagaosa, "Multiferroics of spin origin," Rep. Prog. Phys. **77**, 076501 (2014).
[22]S. Hirose, Y. Iguchi, Y. Nii, T. Kimura, and Y. Onose, "Nonreciprocal microwave response at room temperature in multiferroic Y-type hexaferrite $BaSrCo_2Fe_{11}AlO_{22}$," Appl. Phys. Lett. **121**, 222401 (2022).
[23]Z. Haijun, L. Zhichao, Y. Xi, Z. Liangying, and W. Mingzhong, "Complex permittivity and permeability dependence of $Ba_4Zn_{2-z}Co_zFe_{36}O_{60}$ U-type hexaferrites prepared by citrate solgel on composition, annealing temperature and frequency," Mater. Sci. Eng. B **97**, 160 (2003).
[24]D. Lisjak, V. B. Bregar, and M. Drofenik, "The influence of microstructure on the microwave absorption of Co–U hexaferrites," J. Magn. Magn. Mater. **310**, 2558 (2007).
[25]R. S. Meena, S. Bhattachrya, and R. Chatterjee, "Development of 'tuned microwave absorbers' using U-type hexaferrite," Mater. Des. **31**, 3220 (2010).
[26]S. Kumar, R. S. Meena, and R. Chatterjee, "Microwave absorption studies in Cr-doped Co-U type hexaferrites over 2–18 GHz frequency range," J. Magn. Magn. Mater. **418**, 194 (2016).
[27]T. Honda, Y. Hiraoka, Y. Wakabayashi, and T. Kimura, "Refinement of crystal structure of a magnetoelectric U-type hexaferrite $Sr_4Co_2Fe_{36}O_{60}$," J. Phys. Soc. Jpn. **82**, 025003 (2013).
[28]V. Bovtun, M. Kempa, D. Repček, M. Savinov, J. Buršík, O. Heczko, J. Drahokoupil, and S. Kamba, "Broadband magnetic and dielectric properties of U-type hexaferrite $Sr_4CoZnFe_{36}O_{60}$," J. Magn. Magn. Mater. **589**, 171533 (2023).
[29]D. M. Pozar, *Microwave Engineering*, 4th ed. (John Wiley & Sons, New York, 2012).
[30]H. W. Ott, *Electromagnetic Compatibility Engineering* (John Wiley & Sons, New York, 2009).
[31]See www.southwestmicrowave.com for "Southwest Microwave Microstrip and Coplanar 50 GHz Test Boards."
[32]J. Krupka, "Frequency domain complex permittivity measurements at microwave frequencies," Meas. Sci. Technol. **17**, R55–R70 (2006).
[33]V. Bovtun, V. Pashkov, M. Kempa, S. Kamba, A. Eremenko, V. Molchanov, Y. Poplavko, Y. Yakymenko, J. H. Lee, and D. G. Schlom, "An electrode-free method of characterizing the microwave dielectric properties of high-permittivity thin films," J. Appl. Phys. **109**, 024106 (2011).
[34]V. Bovtun, S. Veljko, A. Axelsson, S. Kamba, N. Alford, and J. Petzelt, "Microwave characterization of thin ferroelectric films without electrodes by composite dielectric resonator," Integr. Ferroelectr. **98**, 53 (2008).
[35]P. Kužel, H. Němec, F. Kadlec, and C. Kadlec, "Gouy shift correction for highly accurate refractive index retrieval in time-domain terahertz spectroscopy," Opt. Express **18**, 15338 (2010).
[36]V. Bovtun *et al.*, "Microwave absorbing and shielding properties of inhomogeneous conductors and high-loss dielectrics," Ferroelectrics **532**, 57–66 (2018).
[37]V. Bovtun, M. Kempa, D. Nuzhnyy, J. Petzelt, O. Borisova, O. Machulianskyi, and Y. Yakymenko, "Composition dependent microwave properties of dielectric-conductor nanocomposites," Phase Transitions **91**, 1027 (2018).
[38]A. R. von Hippel, *Dielectrics and Waves* (The MIT Press, Cambridge, MA, 1966).
[39]S. Kamba, "Soft-mode spectroscopy of ferroelectrics and multiferroics: A review," APL Mater. **9**, 020704 (2021).

[40]J. Chen *et al.*, "Magnetic and and microwave properties of polycrystalline U-type hexaferrite $Ba_4Zn_{2-x}Co_xFe_{36}O_{60}$," J. Magn. Magn. Mater. **496**, 165948 (2020).
[41]D. D. Stancil and A. Prabkhakar, *Spin Waves* (Springer, 2009).
[42]M. S. Sodha and N. C. Srivastava, *Microwave Propagation in Ferrimagnetics* (Springer Science+Business Media, New York, 1981).
[43]S. M. Rezende, *Fundamentals of Magnonics* (Springer Nature Switzerland, 2020).
[44]L. B. Kong, Z. W. Li, L. Liu, R. Huang, M. Abshinova, Z. H. Yang, C. B. Tang, P. K. Tan, R. Deng, and S. Matitsine, "Recent progress in some composite materials and structures for specific electromagnetic applications," Int. Mater. Rev. **58**, 203 (2013).
[45]M.-H. Phan and H.-X. Peng, "Giant magnetoimpedance materials: Fundamentals and applications," Prog. Mater. Sci. **53**, 323 (2008).

Microwave magnetic excitations in U-type hexaferrite $Sr_4CoZnFe_{36}O_{60}$ ceramics

Supplemental material

M. Kempa,[1] V. Bovtun,[1] D. Repček,[1,2] J. Buršík,[3] C. Kadlec,[1] S Kamba[1]

[1]Institute of Physics of the Czech Academy of Sciences, Na Slovance 2, Prague 182 00, Czech Republic

[2]Faculty of Nuclear Sciences and Physical Engineering, Czech Technical University in Prague, Břehová 7, 115 19 Prague, Czech Republic

[3]Institute of Inorganic Chemistry, Czech Academy of Sciences, 250 68 Řež near Prague, Czech Republic

S1. Broadband microwave transmission and absorption.

The full set of *S*-parameters (S_{11}, S_{22}, S_{21}, S_{12}, both magnitude and phase) of the microstrip line (MSL) and coplanar waveguide (CPW) loaded with CoZnU ceramics recorded in the broad frequency range 10 MHz - 50 GHz from 10 K to 390 K shows a reciprocal agreement of the S_{11} and S_{22}, S_{21} and S_{12} spectra. It proves the high quality of the calibration procedure and the reliability of the experiment. For further analysis, the S_{21} and S_{11} spectra were mainly used. As the most sensitive and informative, the following parameters were selected and calculated [1,2,3]:

a) S_{21} magnitude in dB (transmission coefficient *Tr* corresponding to the shielding efficiency *SE* = - *Tr*);

b) input impedance Z_{in} of the MSL or CPW loaded with CoZnU samples, which can be calculated from the S_{11} magnitude in dB (reflection coefficient *R*) as

$$Z_{in} = Z_0 \frac{1+10^{S_{11}/20}}{1-10^{S_{11}/20}}, \quad \text{(s1)}$$

where Z_0 = 50 Ohm is an input impedance of the unloaded, empty MSL or CPW;

c) absorption coefficient *A* which can be calculated as

$$A = 20\log\left(1 - \left|\frac{2Z_{in}}{Z_{in}+Z_0}\right| - \left|\frac{Z_{in}-Z_0}{Z_{in}+Z_0}\right|\right), \quad \text{(s2)}$$

The experimentally recorded S_{11} (S_{11} magnitude in dB is a reflection coefficient R) and S_{21} (S_{21} magnitude in dB is a transmission coefficient Tr) spectra of the CPW loaded with a CoZnU ceramics (see Fig. S1) show multiple resonances with the phase change between –180 and +180 degrees, $R(f)$ maxima above -10 dB and $Tr(f)$ minima below -10÷20 dB. The unloaded CPW is characterized (after the calibration) by the parameter values R < -30 dB, $Tr \approx 0$ dB and S_{21} phase ≈ 0 degrees in the whole frequency range of the experiment. So, all observed resonances are caused by the CoZnU sample coupled with the CPW transmission line. The change and the frequency shift of the observed resonances with temperature are much larger than those caused by the temperature change of the sample and the line sizes, and should be related to the temperature evolution of the sample's electromagnetic properties. The most temperature dependent S_{21} resonance (transmission mode) is marked as T4 in Fig. S1c. *S*-parameters spectra of the MSL loaded with a CoZnU sample slightly differ from those of CPW (due to the different electromagnetic field distribution and sample coupling) but show qualitatively similar temperature changes. This similarity also supports the attribution of the *S*-parameters temperature change to the temperature evolution of the CoZnU electromagnetic properties. *S*-parameters spectra are noisy above 35 GHz, therefore we evaluate data mainly below 35 GHz (see Fig. 1 – Fig. 4 of the main text).

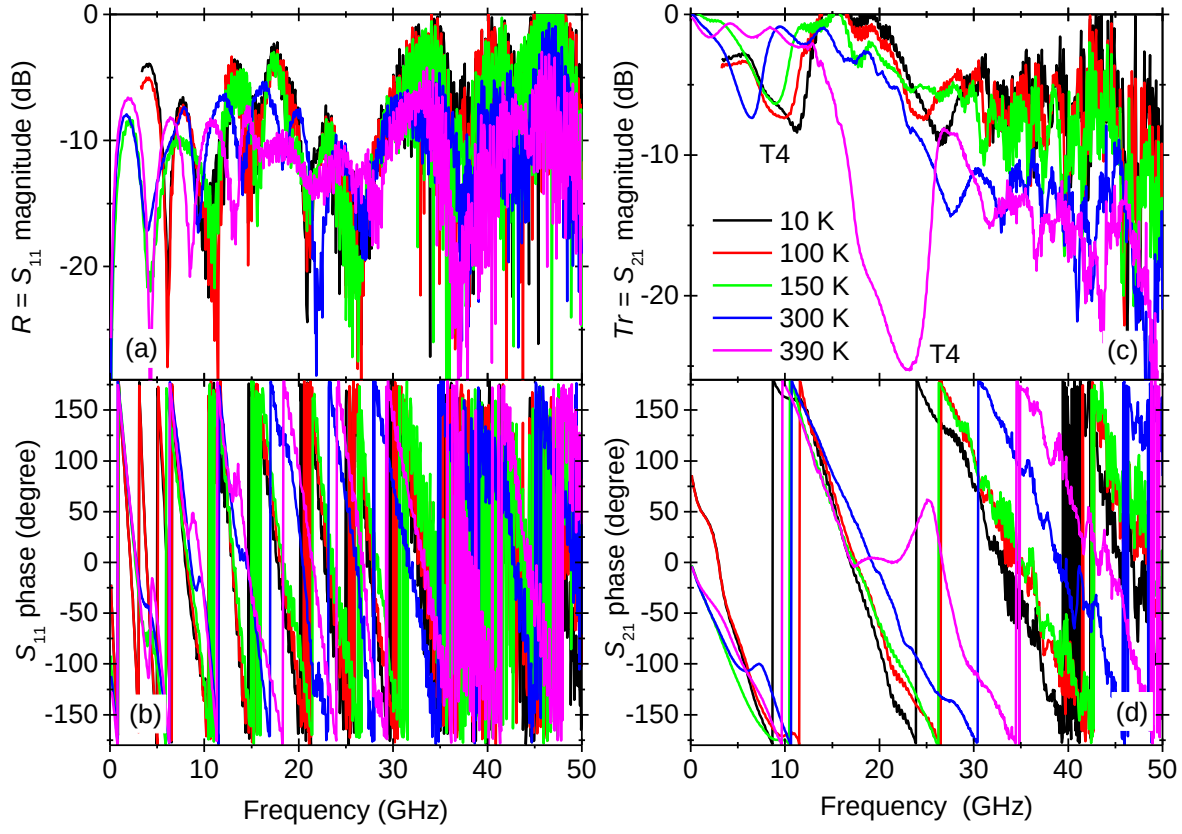

Fig. S1. Recorded broadband spectra of the S_{11} (a, b) and S_{21} (c, d) parameters of the CPW loaded with a CoZnU sample at selected temperatures.

The same set of the transmission modes is observed in both CPW and MSL experiments, with the same CoZnU sample. Moreover, the temperature evolution of the CPW (Fig. 3 in the main text) and MSL (Fig. S3) T-modes is similar, with a remarkable change of their behavior near the CoZnU magnetic phase transitions.

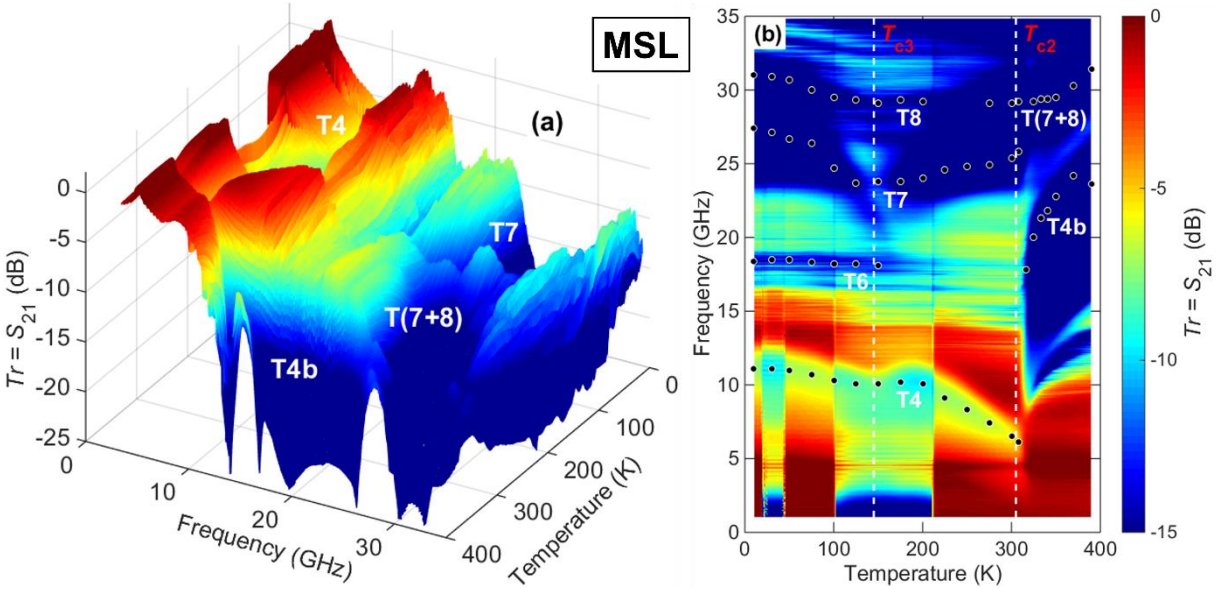

Fig. S2. Temperature-frequency maps of the transmission coefficient *Tr* (S_{21} magnitude) of CoZnU ceramics obtained using the MSL: (a) in 3D view, (b) as a pseudo-3D color map. In (b), points correspond to the main *Tr*(*f*) minima shown in Fig. S3. Temperatures of the phase transitions are marked by dashed lines. Apparent jumps of the *Tr* at several temperatures are instrumental artifacts.

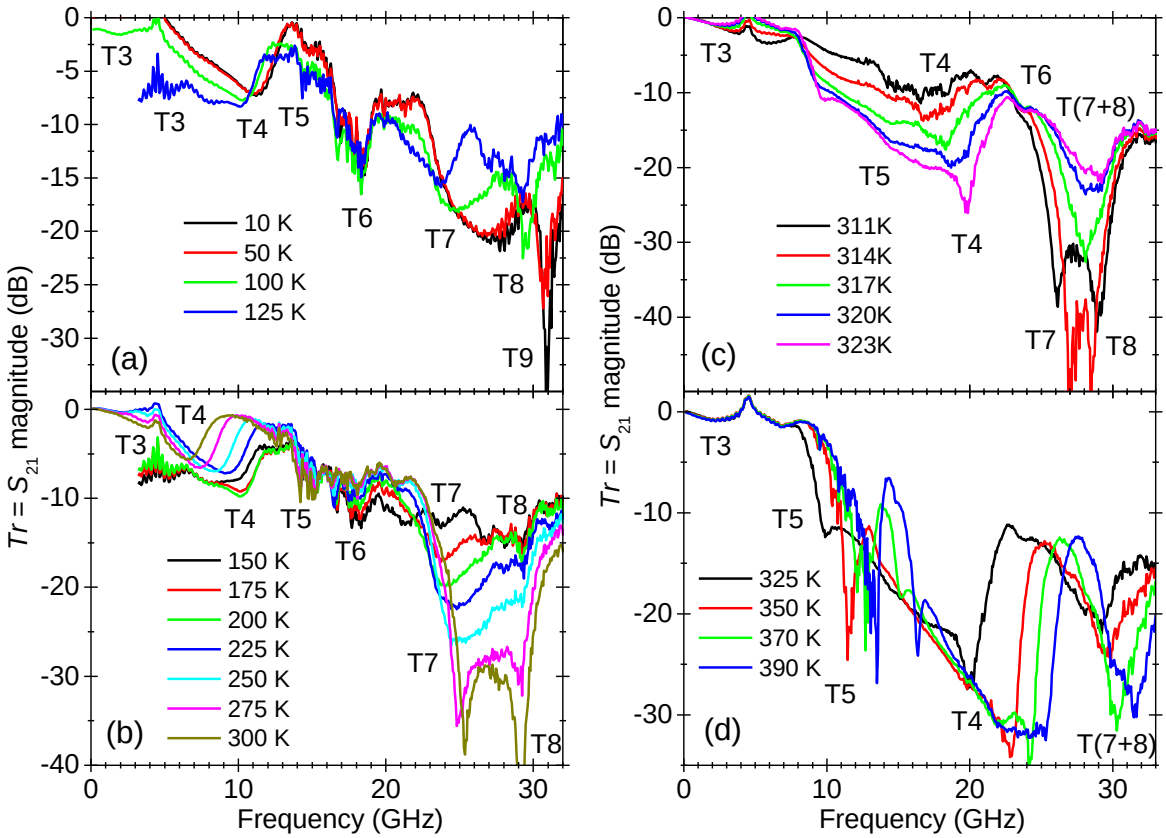

Fig. S3. Broadband spectra of the transmission coefficient *Tr* (S_{21} magnitude) of the MSL loaded with a CoZnU sample at selected temperatures below T_{c3} (a), between T_{c3} and T_{c2} (b), and above T_{c2} temperature (c, d). The main *Tr*(*f*) minima are marked T3 - T9.

In the MSL absorption spectra (Fig. S4), 6 diffuse *A*(*f*) maxima can be recognized below 35 GHz, and they are numbered from A4 to A9 with increasing frequency. These maxima evidence microwave excitations (absorption modes, A-modes). The same system of the A-modes and their similar temperature evolution was derived from both CPW and MSL experiments (except for the A3 mode, which is weak and absent in the MSL spectra). Temperature behavior of the A-modes remarkably changes near the magnetic phase transitions, similar to those of T-modes.

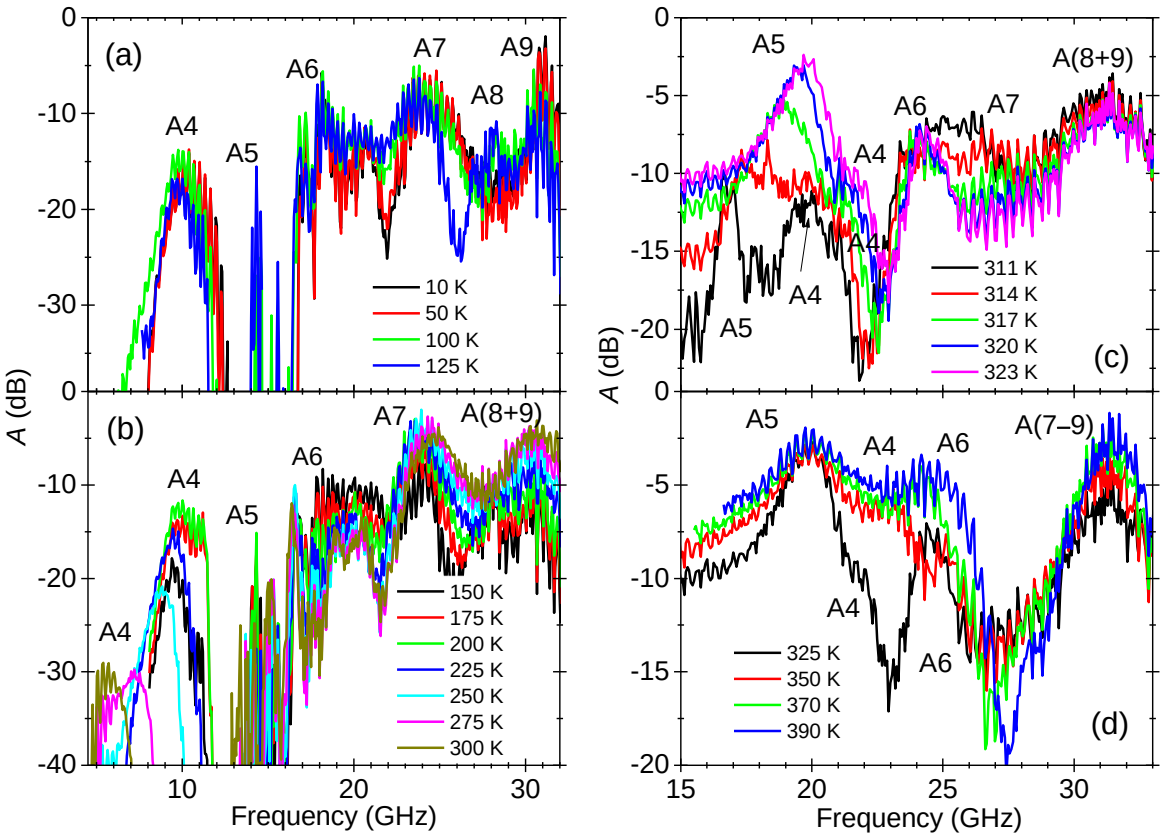

Fig. S4. Broadband spectra of the absorption coefficient A of the MSL loaded with a CoZnU sample at selected temperatures below T_{c3} (a), between T_{c3} and T_{c2} (b), and above T_{c2} (c, d). The main $A(f)$ maxima are marked A4 - A9.

We also analyzed the input impedance spectra $Z_{in}(f)$, calculated using Eq. s1 and shown for CPW in Fig. S5. The spectra for MSL look very similar. The impedance spectra are noisy, similar to the absorption ones (Fig. S4), but less diffused. 7 main $Z_{in}(f)$ maxima seen below 35 GHz are marked Z3 - Z9. These maxima correspond to the transmission minima T3÷T9 (Fig. 2 in the main paper). Sometimes, the $Z_{in}(f)$ maxima are more pronounced, less diffuse, and better separated than the $Tr(f)$ minima. The impedance spectra also confirm a remarkable change of the T-modes behavior near the magnetic phase transition at T_{c2} in the CoZnU ceramics.

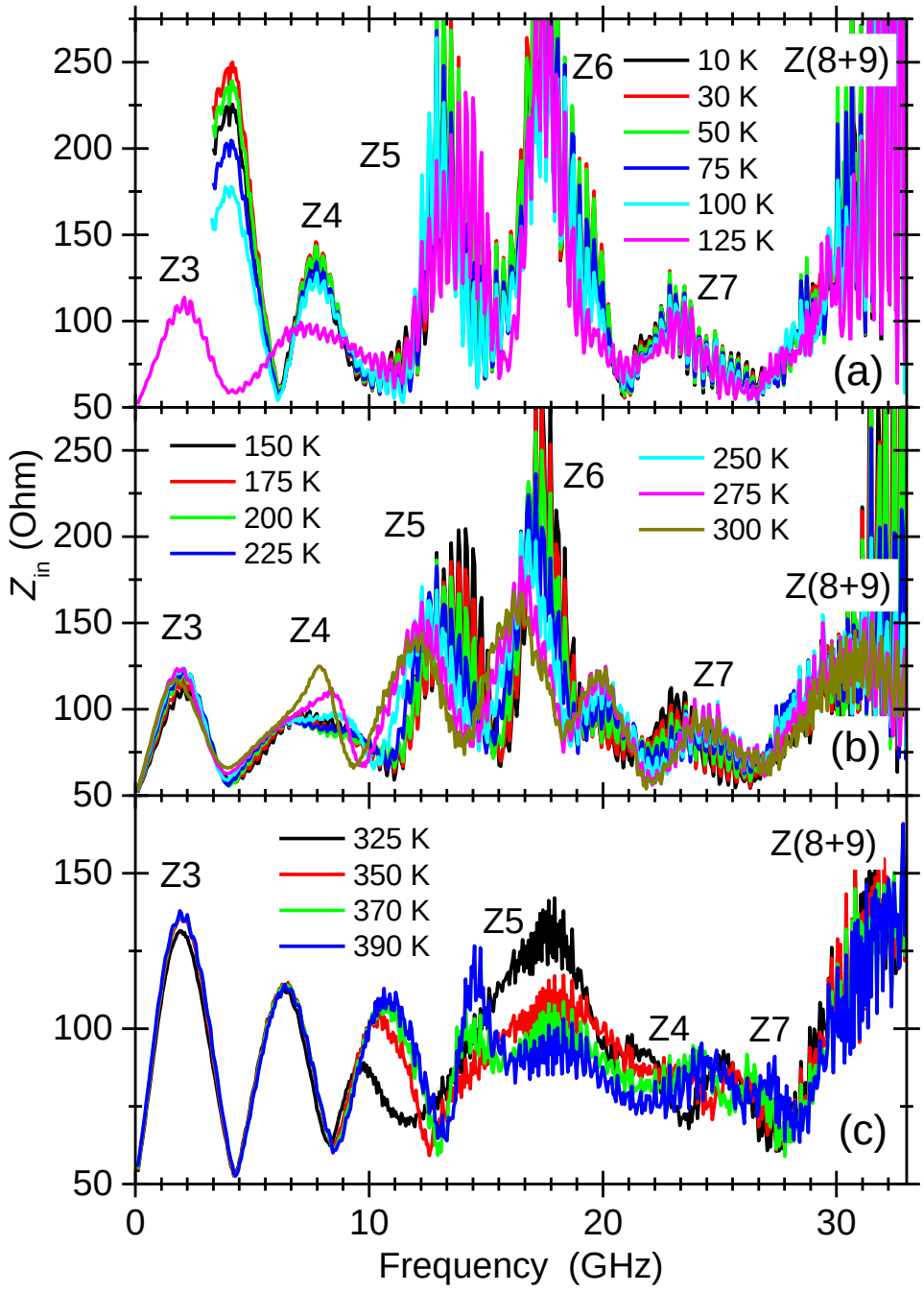

Fig. S5. Broadband spectra of input impedance Z_{in} of the CPW loaded with a CoZnU sample at selected temperatures below T_{c3} (a), between T_{c3} and T_{c2} (b), and above T_{c2} (c). The main $Z_{in}(f)$ maxima are marked Z3 - Z7.

The transmission spectra of the thin cylindrical CoZnU sample, measured as a dielectric resonator (DR) in the shielding cavity [4,5], show a few temperature-dependent resonances (S_{21} maxima) between 8 and 16 GHz with an anomalous behavior near T_{c2} = 305 K

(see temperature-frequency maps in Fig. S6). Opposite to the transmission spectra of CPW or MSL, the DR resonance frequencies (DR-T modes) correspond to the S_{21} maxima, not minima, because the effective transmission is possible only in the case of sufficient coupling at the resonance frequency. The DR-T modes with the most pronounced S_{21} maxima (≥ -40 dB, dark red to brown colors) at ~10 GHz, ~11 GHz, ~13.5 GHz and ~15.5 GHz, and with weak S_{21} maxima (≥ -60 dB, green to yellow colors) are shown also as black points in Fig. S6. Of course, the mean frequencies of the CPW-T and DR-T modes are different, but their temperature behavior is similar. All DR-T modes below 14 GHz slow down toward T_{c2}, similarly to the CPW and MSL T-modes below 22 GHz (Fig. 4 in the main paper). The F4 excitation (CPW-T4) mode, which is characterized by the high absorption and the strongest temperature dependence above T_{c2}, is also shown as a solid line in Fig. S6. It crosses all DR-T modes near T_{c2} with increasing temperature, and the crossing points correspond well to the DR-T mode temperature anomalies.

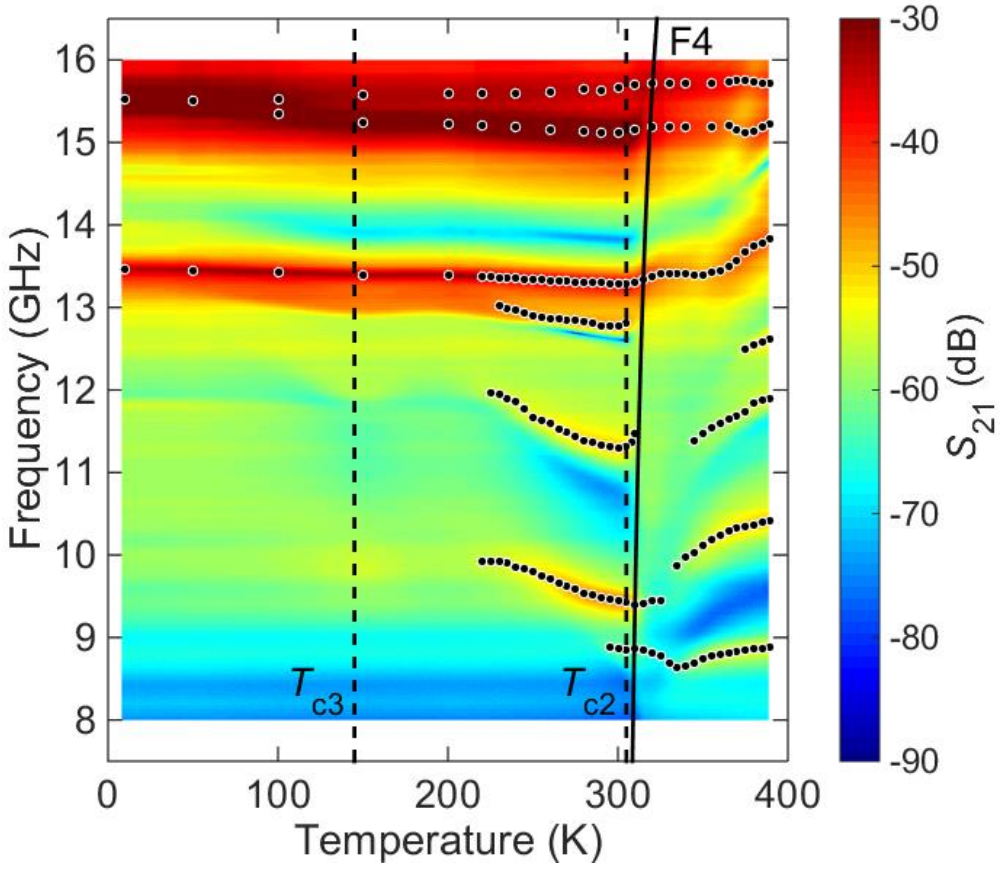

Fig. S6. Temperature-frequency map of the transmission coefficient (S_{21} magnitude) of the CoZnU dielectric resonator. Points correspond to the main $S_{21}(f)$ maxima, solid line near T_{c2} corresponds to the softening of the F4 frequency towards T_{c2} (CPW-T curve from Fig. 4 in the main paper).

S2. THz spectra.

The time-domain THz transmission spectra were measured down to 4 K. The amplitude and phase of the passing wave were determined, and this allowed the complex refractive index $N = (\varepsilon^* \mu^*)^{1/2}$ to be calculated directly [6]. Seven excitations are visible in the THz spectrum, but since we are not sure which are magnetic and which are polar (phonon) excitations, we present in Fig. S7 only the components of the complex refractive index N and not the complex dielectric permittivity ε^* and magnetic permeability μ^* spectra. However, we estimate from the shape of the excitations which ones are magnons and which are phonons. We label their frequencies in Fig. S7 with arrows.

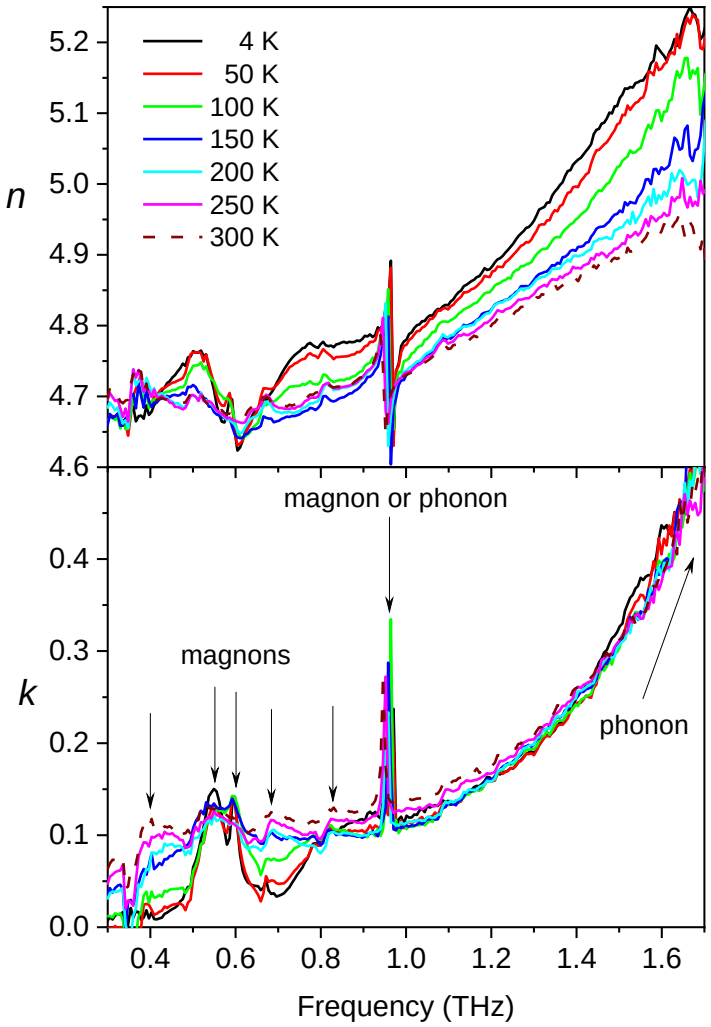

Fig. S7. Temperature dependence of the complex refractive index $N=n+ik$ in the THz region. The frequencies of the magnetic and of the lattice excitations are marked.

References.

[1] H. W. Ott “Electromagnetic Compatibility Engineering”, I. Wiley & Sons, New York, 2009.

[2] V. Bovtun, M. Kempa, D. Nuzhnyy, J. Petzelt, O. Borisova, O. Machulianskyi, Y. Yakymenko "Microwave absorbing and shielding properties of inhomogeneous conductors and high-loss dielectrics", Ferroelectrics **532**, 57 (2018).

[3] V. Bovtun, M. Kempa, D. Nuzhnyy, J. Petzelt, O. Borisova, O. Machulianskyi, Y. Yakymenko “Composition dependent microwave properties of dielectric-conductor nanocomposites”, Phase Transitions **91**, 1027 (2018).

[4] J. Krupka "Frequency domain complex permittivity measurements at microwave frequencies", Meas. Sci. Technol. **17**, R55 (2006).

[5] A. Maia, C. Kadlec, M. Savinov, R. Vilarinho, J. A. Moreira, V. Bovtun, M. Kempa, M. Míšek, J. Kaštil, A. Prokhorov, J. Maňák, A. A. Belik, S. Kamba, Can the ferroelectric soft mode trigger an antiferromagnetic phase transition? J. Eur. Ceram. Soc. **43**, 2479 (2023).

[6] P. Kužel, H. Němec, F. Kadlec, and C. Kadlec. Gouy shift correction for highly accurate refractive index retrieval in time-domain terahertz spectroscopy. Opt. Express **18** 15338 (2010).